JOURNAL OF GEOPHYSICAL RESEARCH, VOL. 97, NO. B1, PAGES 449–478, JANUARY 10, 1992

Great Thrust Earthquakes and Aseismic Slip Along the Plate Boundary of the Makran Subduction Zone

DANIEL E. BYRNE[1] AND LYNN R. SYKES

Lamont-Doherty Geological Observatory and Department of Geological Sciences, Columbia University Palisades, New York

DAN M. DAVIS

Department of Earth and Space Sciences, State University of New York at Stony Brook

The Makran subduction zone of Iran and Pakistan exhibits strong variation in seismicity between its eastern and western segments and has one of the world's largest forearcs. We determine the source parameters for 14 earthquakes at Makran including the great (M_W 8.1) earthquake of 1945 (the only instrumentally recorded great earthquake at Makran); we determine the loci of seismic and aseismic slip along the plate boundary, and we assess the effects of the large forearc and accretionary wedge on the style of plate boundary slip. We apply body waveform inversions and, for small-magnitude events, use first motions of P waves to estimate earthquake source parameters. For the 1945 event we also employ dislocation modeling of uplift data. We find that the earthquake of 1945 in eastern Makran is an interplate thrust event that ruptured approximately one-fifth the length of the subduction zone. Nine smaller events in eastern Makran that are also located at or close to the plate interface have thrust mechanisms similar to that of the 1945 shock. Seaward of these thrust earthquakes lies the shallowest 70-80 km of the plate boundary; we find that this segment and the overlying accretionary wedge remain aseismic both during and between great earthquakes. This aseismic zone, as in other subduction zones, lies within that part of the accretionary wedge that consists of largely unconsolidated sediments (seismic velocities less than 4.0 km/s). The existence of thrust earthquakes indicates that either the sediments along the plate boundary in eastern Makran become sufficiently well consolidated and dewatered about 70 km from the deformation front or older, lithified rocks are present within the forearc so that stick-slip sliding behavior becomes possible. This study shows that a large quantity of unconsolidated sediment does not necessarily indicate a low potential for great thrust earthquakes. In contrast to the east, the plate boundary in western Makran has no clear record of historic great events, nor has modern instrumentation detected any shallow thrust events for at least the past 25 years. Most earthquakes in western Makran occur within the downgoing plate at intermediate depths. The large change in seismicity between eastern and western Makran along with two shallow events that exhibit right-lateral strike-slip motion in central Makran suggest segmentation of the subduction zone. Two Paleozoic continental blocks dominate the overriding plate. The boundary between them is approximately coincident with the transition in seismicity. Although relative motion between these blocks may account for some of the differing seismic behavior, the continuity of the deformation front and of other tectonic features along the subduction zone suggests that the rate of subduction does not change appreciably from east to west. The absence of plate boundary events in western Makran indicates either that entirely aseismic subduction occurs or that the plate boundary is currently locked and experiences great earthquakes with long repeat times. Evidence is presently inconclusive concerning which of these two hypotheses is most correct. The presence of well-defined late Holocene marine terraces along portions of the coasts of eastern and western Makran could be interpreted as evidence that both sections of the arc are capable of generating large plate boundary earthquakes. If that hypothesis is correct, then western Makran could produce a great earthquake or it could rupture as a number of segments in somewhat smaller-magnitude events. Alternatively, it is possible that western Makran is significantly different from eastern Makran and experiences largely aseismic slip at all times. A knowledge of the velocity structure and nature of the state of consolidation or lithification of rocks at depth in the interior portion of the forearc of western Makran should help to ascertain whether that portion of the plate boundary moves aseismically or ruptures in large to great earthquakes. A resolution of this question has important implications for seismic hazard not only for western Makran but also for other margins, such as the Cascadia subduction zone of western North America, where historical thrust events have not occurred.

INTRODUCTION

Plate motion in the form of earthquakes may occur in a variety of ways at subduction zones. Some margins produce frequent thrust earthquakes of only moderate to large size (e.g., several parts of the Mexican subduction zone), some experience great events separated by periods of little moderate-size activity (e.g., southern Chile), while still others have experienced no known plate boundary earthquakes during historic times (e.g., Cascadia, Java, southern Lesser Antilles), making it difficult to ascertain whether they subduct aseismically or undergo great earthquakes separated by periods exceeding the historic record. The Makran subduction zone is unusual in several respects: the eastern and western halves of Makran exhibit very different patterns of seismicity, have historic records with and apparently without great events, respectively, and both segments are the site of one of the world's largest forearc

1 Now at Instituto de Geofisica, Universidad Nacional Autónoma de México, Cindad Universitaria, Delegación de Coyoacar.

Paper number 91JB02165.
0148-0227/92/91JB-02165$05.00

regions. The seaward 70 km of the forearc consists of more recently accreted, unconsolidated and semiconsolidated sediments that have low seismic velocities and high pore fluid pressures [e.g., *White*, 1982; *Fowler et al.*, 1985].

A number of other convergent margins with unusual or unknown seismic behaviors contain relatively large volumes of young sediment. Unconsolidated sediment exhibits higher coefficients of friction at higher slip velocities (so-called velocity-strengthening behavior), causing a resistance to the accelerating slip associated with earthquakes [e.g., *Marone and Scholz*, 1988]. This stable frictional slip behavior is manifested as an aseismic region along the shallow portions of some active strike-slip fault zones. In California this zone of slip is typically confined to the upper few kilometers of active faults. Similarly, aseismic slip is associated with the presence of unconsolidated sediments along the shallowest part of plate boundaries at subduction zones [*Byrne et al.*, 1988]. For the subduction zones examined by *D. E. Byrne, L. R. Sykes and D. M. Davis* (manuscript in preparation) this zone of aseismic slip extends beneath the region of the accretionary wedge with seismic velocities less than about 4.5 km/s. A transition to seismic slip occurs either as the young sediment becomes more consolidated or as older more lithified rocks are encountered. The depth to which aseismic conditions might persist along a fault within sediment is not well known. Hence the presence of large volumes of sediment may influence the potential to generate great earthquakes at Makran and at subduction zones with similar conditions such as Cascadia and the southern Lesser Antilles.

The Makran region of southern Pakistan and southeastern Iran is a 1000-km section of the Eurasian-Arabian plate boundary (Figures 1 and 2) where consumption of oceanic crust has occurred continuously since the Early Cretaceous along a north dipping subduction zone [e.g., *Farhoudi and Karig*, 1977; *Sengör et al.*, 1988]. Makran remains a sparsely populated and remote region with a relatively low level of seismicity and infrequent great earthquakes. The repeat times and focal parameters of Makran earthquakes have been poorly documented because so few moderate ($M_S \geq 5.5$) or large ($M_S \geq 7.0$) earthquakes are known to have occurred there. The only instrumentally recorded great ($M_S > 7.7$) earthquake at Makran occurred in 1945, but its source parameters were not determined prior to our work. Thus the seismic behavior of the Makran subduction zone has remained largely unknown.

In this paper we analyze available data including seismograms from a number of events, seismicity, seismic reflection and refraction data, and onshore geology to determine the seismic behavior of the Makran subduction zone. New focal solutions are presented for 13 earthquakes beginning with an analysis of the great (M_W 8.1) event of 1945 (Figure 3). The historic data for the 1945 event are of poor quality by modern standards. They do not allow a detailed analysis of the rupture history, but do permit us to determine the focal solution, source time function, approximate rupture direction, and magnitude. Below we describe our solution for this and for other events and discuss the seismotectonics of Makran. We also consider the implications for the modes of slip along the plate boundary and for seismic hazard at Makran.

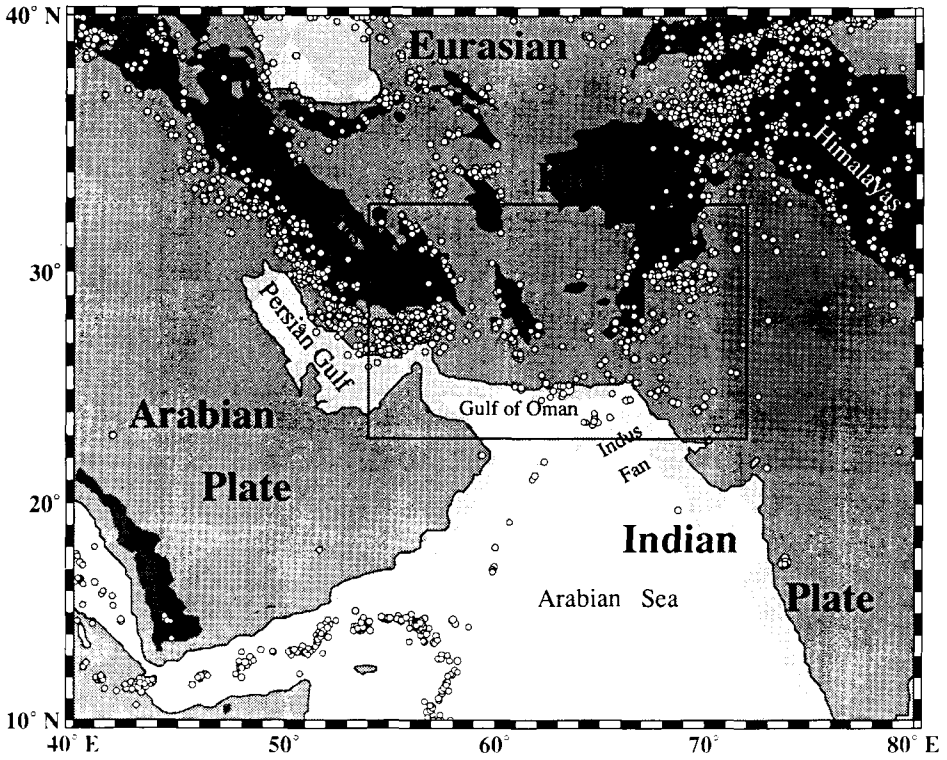

Fig. 1. Earthquakes of the Makran subduction zone and surrounding region (open circles) from the International Seismic Summary (ISS) catalogue between 1944 to 1987 of m_b greater than 4.7. Symbol size is proportional to magnitude. Elevation is shown by gray shades with 1500-m contour interval; darker gray indicates higher elevation. Seismicity and topography delineate active plate boundaries. Box encloses the Makran region shown in detail in Figure 2. Note lower level of seismicity along Makran segment of the Eurasian-Arabian plate boundary relative to the section farther west and the decrease in seismicity along the coast of Makran from east to west.

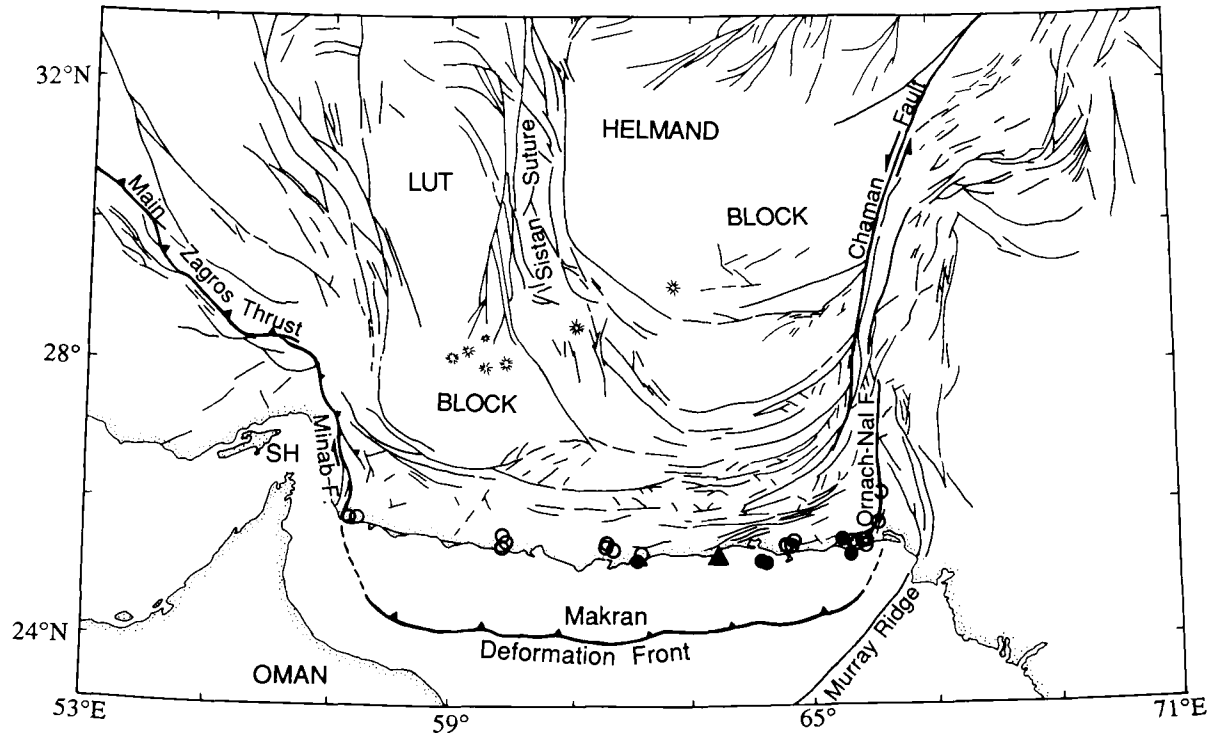

Fig. 2. Faults (solid lines) and major tectonic features of Makran subduction zone [after *Haghipour et al.*, 1984]. Arabian plate is being subducted beneath Eurasian plate along deformation front (teeth on overriding plate). Epicenter of 1945 great earthquake is shown as solid triangle. Mud volcanoes along the coast are shown by open circles; those activated by 1945 event are shown as solid circles. Calc-alkaline volcanoes are shown by concentric, radiating spokes. Lut and Helmand blocks are older micro continental fragments separated by Sistan suture zone. SH is Strait of Hormuz.

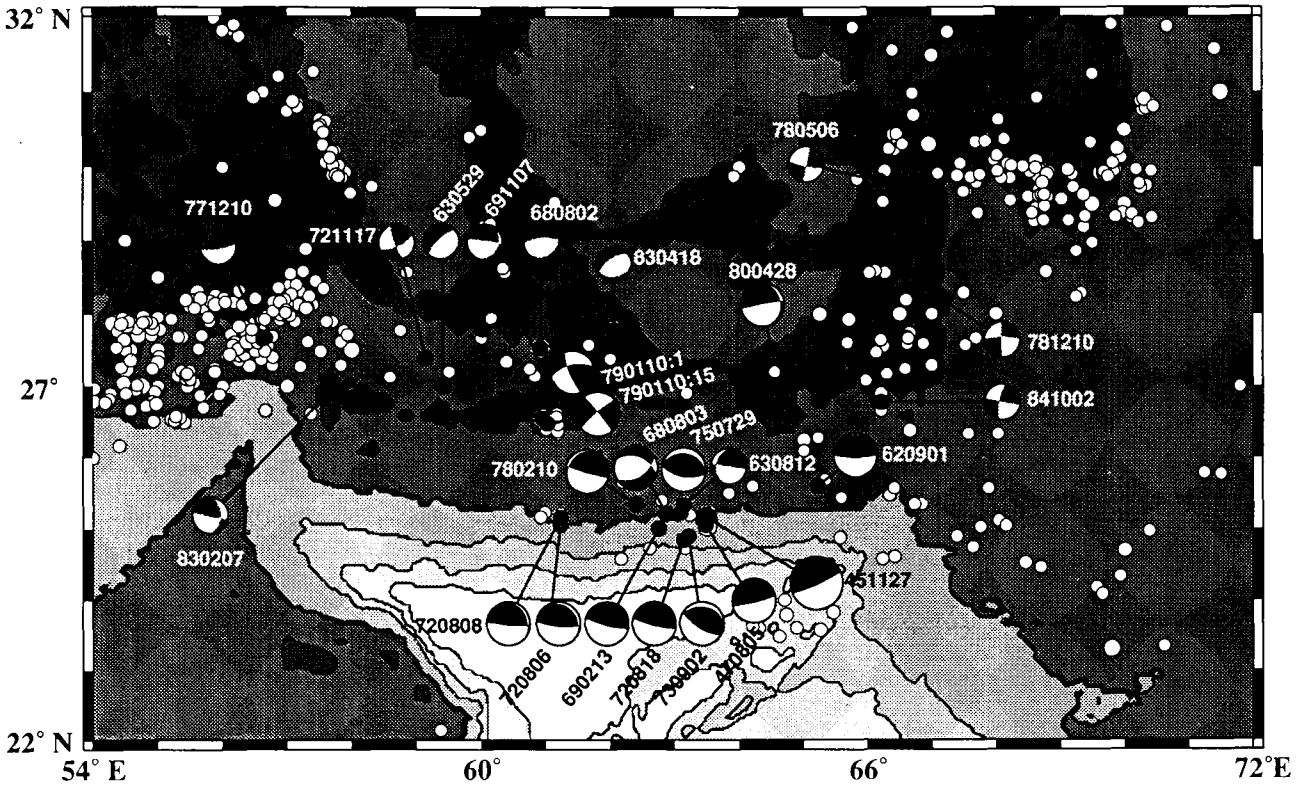

Fig. 3. Focal mechanisms of Makran earthquakes determined in this study (black and white) and in previous studies (gray and white). Lower hemisphere projections with dark compressional quadrants. Source parameters are summarized in Tables 1 and 2. Seismicity of Figure 1 also shown by open circles. Topography is indicated by gray shades with 1000-m contour interval; darker shades correspond to higher elevations. Thick contour is the coast. Note sharp contrast between presence of seismicity and focal mechanisms in eastern Makran and their absence in western Makran. That transition aligns with the north trending ridge of the Sistan suture (Figure 2).

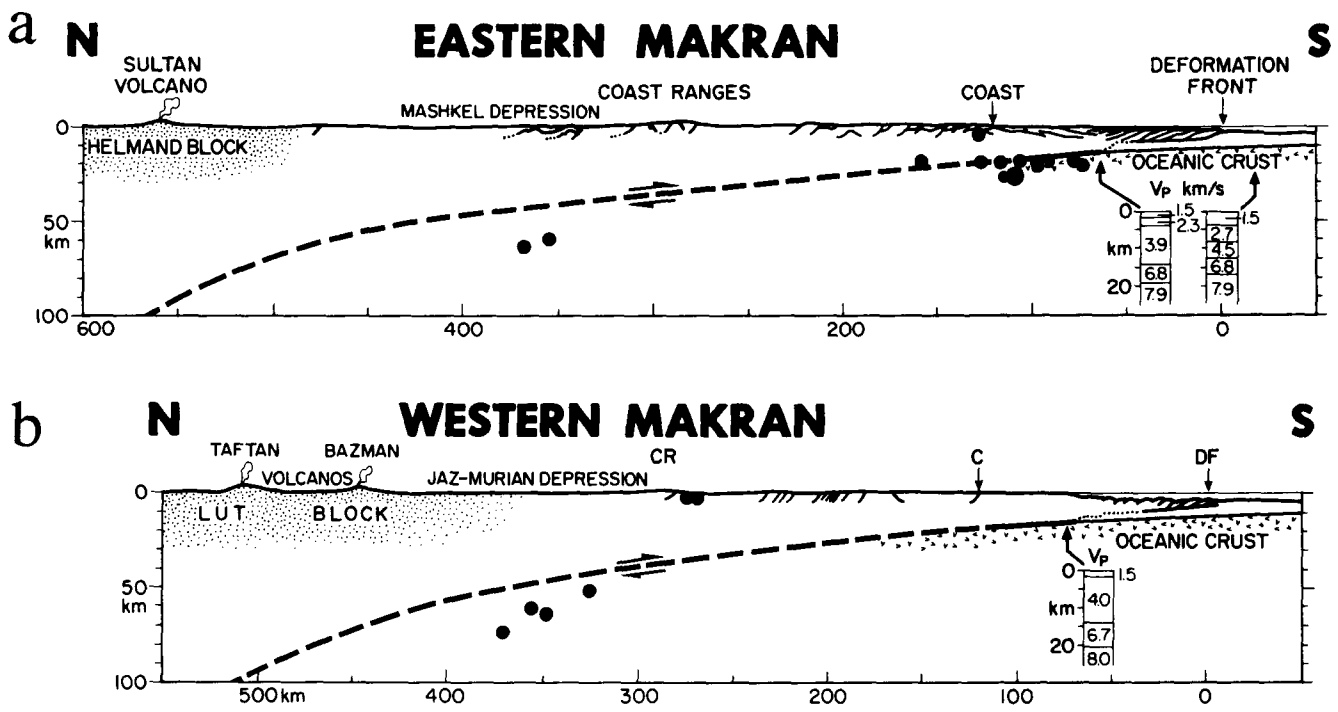

Fig. 4. North-south cross-sections across (*a*) eastern Makran (near 63.5°E) and (*b*) western Makran (near 59.5°E) showing generalized geologic structure, generalized topography, location of the plate boundary (dashed where inferred), and characteristic seismicity. Earthquakes listed in Tables 1 and 2 are projected into the sections: those east of 61°E onto Figure 4*a*, those to the west onto Figure 4*b* volcanic centers are also projected into sections. Main differences between eastern and western Makran include absence of coastal earthquakes in western Makran and greater distance between volcanic arc and deformation front in eastern Makran. Note that plate interface steps down through sedimentary section in southernmost 70 km of overriding plate in both Figures 4*a* and 4*b*. Interval velocities determined offshore also shown. Generalized structure and velocity information in Figure 4*a* is based on data from *Hunting Survey Corporation* [1960], *Ahmed* [1969], *Harms et al.* [1984], *White* [1984], *White and Louden* [1982], *Minshull and White* [1989], *Platt et al.* [1988], and *Platt* [1990], and in Figure 4*b* from *White and Klitgord* [1976], *White and Ross* [1979], *Niazi et al.* [1980], *McCall and Kidd* [1982], and *Haghipour et al.* [1984].

We find that the Makran subduction zone exhibits a strong segmentation between east and west in its seismic behavior. The plate boundary in eastern Makran ruptures in large and great thrust earthquakes (1945) and currently experiences small- and moderate-sized thrust earthquakes (Figure 4*a*). In contrast, western Makran exhibits no well-documented great earthquakes in historic times, and modern instrumentation has not detected any shallow events along the plate boundary (Figure 4*b*). We find that aseismic conditions persist downdip along the shallowest 70-80 km of the plate boundary (i.e., depths shallower than about 17 km) across the entire margin (Figures 4 and 5). The seaward aseismic region coincides with the youngest portion of the accretionary wedge where low-velocity sediments are observed. Seismic slip extends updip to near the coast in eastern Makran. How far updip seismic slip occurs in western Makran, and even whether the plate boundary there moves in large earthquakes, is presently unresolved. The pressures to which unconsolidated sediment (and thus an aseismic zone) may persist downdip at any subduction zone depend on an often poorly known set of parameters that determine the rate of dewatering, including permeability, porosity, lithology, and strain rate. The mechanical behavior of either those sediments (dependent upon all of the factors that control compaction and lithification) or the possible presence of older, strongly lithified rocks at depth in forearcs governs whether or not plate boundary slip at any point is seismic.

TECTONIC SETTING OF MAKRAN SUBDUCTION ZONE AND STRUCTURE OF THE OVERRIDING PLATE

The southern border of much of the Eurasian plate is a part of the Tethyside collage of suture belts; its development is described in detail by *Sengör et al.* [1988] (see their Figure 20). The overriding plate at Makran is dominated by two accreted terranes of Gondwanan origin, the Lut block, a southern section of the Central Iranian Microcontinent, and the Helmand or Afgan block (Figure 2). These blocks were once separated by an arm of the Neo-Tethys that was subducted to the east beneath the Helmand block leaving the north trending Sistan suture zone [*Tirrul et al.*, 1983]. All of the oceanic crust between these blocks is thought to have been subducted by middle Eocene. North directed subduction of Neo-Tethyian oceanic crust continued beneath the southern margins of both these blocks since Late Cretaceous, defining the Makran subduction zone. During the Eocene an accelerating rate of accretion began along the southern edge of these blocks presumably related to the influx of sediment as the collision of India caused extensive uplift east of Makran. Such accretion has extended the upper plate by more than 300 km (Figures 2 and 4). That growth has caused wide separation between the volcanic arc and the deformation front [*McCall and Kidd*, 1982].

Today oceanic crust of the Arabian plate continues to be

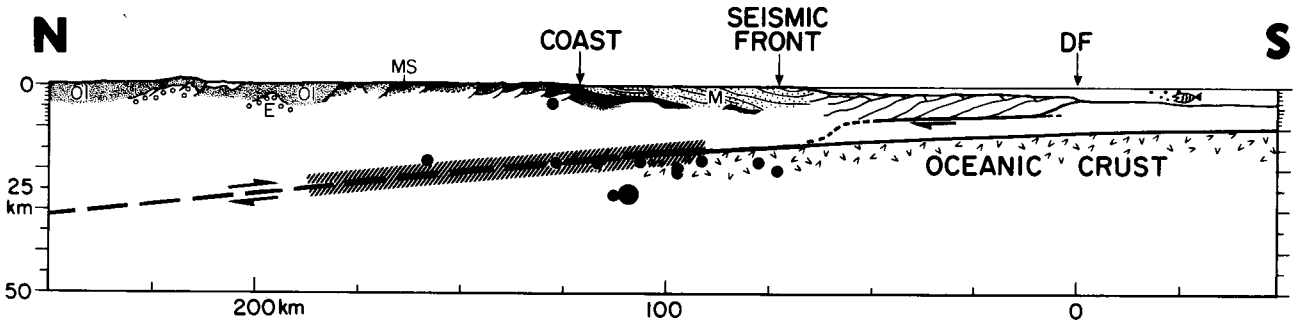

Fig. 5. A more detailed cross section of structure and seismicity of coastal region of eastern Makran (63.5°E) in which the 1945 earthquake occurred. Dots are earthquake hypocenters. Seismic front indicates seaward limit of earthquakes. Maximum inferred rupture along the plate boundary during 1945 event is shown by broad line segment. Note change in slope of seafloor approximately 70 km north of deformation front. DF indicates the deformation front. Ol indicates rock accreted in the Oligocene, E, Eocene, M, Miocene shelf sediment, and MS, Miocene slope sediment. Data sources same as Figure 4*a*.

consumed along the Makran subduction zone with an azimuth of N10°E. The convergence velocity estimated by *DeMets et al.* [1990] increases from 36.5 mm/yr near the Strait of Hormuz to 42.0 mm/yr at the eastern boundary of Makran. That estimate is the best available, but it relies on the assumption of completely rigid plate motion. The plate collisions occurring along the southern boundary of the Eurasian plate, however, occupy an extremely broad zone of diffuse tectonic activity that extends as far north as central Asia, Afghanistan, and western China [e.g., *Molnar*, 1988]. Thus a significant (but unknown) fraction of the convergence between the Arabian and Eurasian plates probably is accommodated by deformation well to the north of the Makran subduction zone. As described below, the original segmentation of the upper plate between the Lut and Helmand blocks is still expressed in physiography and in seismicity. These blocks compose the arcward regions of the overriding plate (Figure 4); some relative motion between them still appears to influence the present-day tectonics of Makran. Segmentation between eastern and western Makran, however, is not observed along the modern accretionary wedge nor at the deformation front, indicating that oceanic crust is currently being subducted steadily along the entire arc. The age of the crust of the Gulf of Oman (Figure 1) cannot be uniquely determined from the magnetic reversal time scale because the crust is devoid of magnetic anomalies and is presumed to have formed during the Cretaceous quiet period (79-108 Ma) [*Coleman*, 1981]. Estimates from heat flow measurements place the age at 70-100 Ma [*Hutchison et al.*, 1981]. The Semail Ophiolite in Oman may be part of the same crust and has been dated at 86-95 Ma from biostratigraphy [*Tippit et al.*, 1981] and at 93.5-97.9 Ma from U-Pb dating [*Tilton et al.*, 1981]. These data suggest that the age of the seafloor near the trench is between 70 and 100 Ma and probably lies close to 95 Ma.

The boundaries of the the Makran subduction zone are all rather complex tectonic features. Major transpressional strike-slip systems, the Ornach-Nal and Chaman fault zones, form the eastern boundary of Makran and accommodate the motion between the Eurasian plate and the western part of the Indian plate (Figure 2). Sinistral slip along these fault systems and thrusting within the ranges to the east of those fault zones are well documented and are associated with several destructive earthquakes [*Quittmeyer and Jacob*, 1979]. To the south the Murray Ridge (Figure 2) delineates part of the Arabian-Indian plate boundary [*Gordon and DeMets*, 1989]. The ridge extends from the northern tip of the Owen fracture zone to the eastern corner of Makran. It consists of a volcanic ridge of seamounts currently experiencing uplift [*White*, 1983]. The topography of the ridge separates two distinct basins: the Gulf of Oman to the northwest and the Arabian Sea to the southeast (Figure 1). The Murray Ridge has been the locus of small earthquakes with right-lateral strike-slip and normal faulting motion [*Banghar and Sykes*, 1969; *Quittmeyer and Kafka*, 1984]. The Minab fault system (Figure 2) joins the western edge of Makran with the northwesterly trending compressional zone of the Zagros fold-and-thrust belt [*White and Ross*, 1979]. The eastern edge of the Straits of Hormuz marks the boundary between continental crust of the Arabian shield and oceanic crust of the Gulf of Oman [*White and Ross*, 1979]. The underthrusting of these different types of crust beneath the Eurasian margin may account for some of the marked difference in tectonic styles between the Zagros and Makran [e.g., *Farhoudi and Karig*, 1977; *Kadinsky-Cade and Barazangi*, 1982]. The contrast between the accretion of a thick pile of trench sediments in the Makran and overthrusting on two distinct, thick evaporite layers in the Zagros [*Farhoudi*, 1978] must also contribute to the very different styles of faulting near the southern shores of these two areas.

Young, low-velocity sediments 6-7 km thick blanket the Gulf of Oman in front of the Makran deformation front [*White*, 1982; *Fowler et al.*, 1985]. Erosion of the western Himalayan Mountains, ongoing since middle Eocene, contributes much of the largely fine-grained sediment to the Indus Fan [*Milliman et al.*, 1984] and to the post-Eocene sediment accreted along the Makran margin [*Harms et al.*, 1984]. The Murray Ridge currently blocks the transport of Indus sediment to the Gulf of Oman [*Stewart et al.*, 1965]; however, that sediment ponding is a recent effect caused by uplift of the ridge [*White*, 1983; *Collier and White*, 1990]. Other significant sources of sediment within the Gulf of Oman are erosion from Makran itself associated with coastal uplift [*McCall and Kidd*, 1982] and dust-bearing winds from Arabia [*Stewart et al.*, 1965]. Thus the bulk of the sediment within the Gulf of Oman and that accreted at Makran is largely fined-grained, terrigenous sand and clay.

The uppermost 2.5 km of the sediments on the Arabian plate are currently being accreted to the upper plate at the deformation front [*White*, 1979, 1982] while the rest of the

sediment is carried beneath the deformation front without significant deformation (Figures 4 and 5) [*Minshull and White*, 1989]. Young sediments accreted to the upper plate experience rapid initial consolidation and dewatering in the frontal fold [*Minshull and White*, 1989]. Farther arcward little additional deformation or dewatering appears to occur for approximately 70 km [*White*, 1982; *Fowler et al.*, 1985]. *Fowler et al.* [1985] find very low seismic velocities within the outermost 70 km of the upper plate, nearly all less than 4.0 km/s. These low velocities provide further evidence for relatively low states of consolidation within these accreted sediments. The constant and nearly flat slope of the accretionary wedge in this region indicates that the downgoing plate slips along weak horizons within the sediments and encounters very little resistance [*White*, 1982; *Davis et al.*, 1983]. The extremely small taper of the frontal 70 km of the accretionary wedge suggests that pore fluid pressures along the décollement must approach lithostatic [*Davis et al.*, 1983] or possibly even exceed it [*Platt*, 1990].

Folding and rapid uplift commencing 70 km from the deformation front (Figure 5) result in an abrupt increase in the slope of the accretionary wedge [*White*, 1982]. Such an increase may be caused by increased shear strength along the décollement and/or lower shear strength within the upper plate. Alternatively, it may simply be a surficial manifestation of large-scale ramping at depth caused by the basal detachment stepping downsection (causing underplating of sediments to the upper plate). Much of the sediment subducted past the deformation front is thought to be underplated [*Platt et al.*, 1985; *White and Louden*, 1983]. *Platt et al.* [1985] note a transition in nearshore geology from Oligocene to mid-Miocene abyssal plain turbidites to Miocene-Pliocene shelf sediments that occurs over less than 2 km of stratigraphic thickness. That change implies far more uplift or thickening than can be accounted for by observed stratigraphic or structural features, leading *Platt et al.* [1985] to suggest that the thickening is caused by large-scale underplating of sediment in which the décollement steps down to lower stratigraphic levels. *White* [1982] suspects that thrust faults associated with this thickening extend down to oceanic basement. Because the décollement typically forms along the stratigraphic layer with least shear strength [e.g., *von Huene*, 1984], the change of the décollement to deeper stratigraphic levels, as well as the venting of fluids from numerous large mud volcanoes and mud ridges [*Snead*, 1964], provides evidence that the upper plate experiences a significant increase in dewatering and strengthening beginning approximately 70 km from the deformation front. The idea that there is a transition in the nature of resistance to plate motion is also supported by the onset of plate boundary seismicity just arcward of the change in slope (Figure 5). The plate boundary in this transitional region is situated in or near oceanic crust at a depth of approximately 17 km.

North of the coastline up to at least the Makran Coastal Ranges (Figure 4) the overriding plate is composed of additional accreted flysch and ophiolites. These rocks become increasingly older, deformed, and lithified in a northward direction. Farther north broad depressions occur in which the geology is obscured by fields of sand dunes [*Hunting Survey Corporation*, 1960]. The accreted rocks abut the Lut and Helmand blocks within or north of these depressions [e.g., *McCall and Kidd*, 1982]. Although accreted rocks make up more than 300 km of the overriding plate at Makran, only the southernmost 70 km appears to retain a relatively unconsolidated state characteristic of modern, young accretionary wedges at other convergent margins.

The distance between the volcanic arc and the deformation front is approximately 400 km in western Makran and grows to nearly 600 km (Figure 4) in eastern Makran [*Jacob and Quittmeyer*, 1979]. The depth of the plate boundary north of the coastline is not well defined because the level of seismicity there is quite low. We infer its approximate position (Figure 4) from the locations of intermediate-depth earthquakes and from the locus of the volcanic arc (known to occur where the downgoing plate reaches depths of approximately 100 km [*Isacks and Barazangi*, 1977]). The plate interface across both eastern and western Makran maintains a shallow dip for hundreds of kilometers thereby producing an exceptionally broad downdip width of the shallow plate interface.

Earthquakes of the Makran Subduction Zone

The level of seismicity in Makran is quite low. Those earthquakes that do occur are generally small, with few teleseismic events larger than magnitude 5, and large or great earthquakes are uncommon. A number of focal mechanisms have been determined for events with magnitudes around 6 [e.g., *Jacob and Quittmeyer*, 1979; *Jackson and McKenzie*, 1984; *Quittmeyer and Kafka*, 1984; *Laane and Chen*, 1989]. Most of these events occur as bending-related earthquakes at intermediate depths within the downgoing plate (Tables 1 and 2). Events that may lie on the plate interface occur near the coast at shallow depths exclusively in central and eastern Makran. Nearly all of these events have magnitudes less than m_b 4.5. Few of their focal solutions have previously been determined [*Quittmeyer and Kafka*, 1984; *Jackson and McKenzie*, 1984].

We examined all known Makran earthquakes along the coastal band of seismicity that are potentially associated with motion along the plate boundary. We determined focal parameters for events that were sufficiently large so as to produce useful teleseismic bodywaves (approximately m_b 4.8) and estimated depths from the arrival times of phases reflected from the Earth's surface (Table 1). We employed the body waveform inversion technique of *Nábělek* [1984] for larger events (generally greater than m_b 5.2) and used first motions of P waves recorded by the World-Wide Standard Seismic Network (WWSSN) for smaller events.

In this study we discuss small earthquakes and report body wave magnitudes, m_b (computed from amplitudes of short-period P waves). We also consider larger earthquakes for which the body wave magnitude saturates. For large and great events we use the surface wave magnitude, M_S (based on 20-s Rayleigh wave amplitudes), and the moment magnitude, M_W (based on the scalar seismic moment, M_O), respectively. We also give the seismic moments we estimate from our waveform analyses (Table 1). Scalar seismic moment is defined as the product of rupture area, average rigidity, and average slip; it may also be derived from the spectral amplitude at 0 Hz or from body or surface wave analyses that are used to estimate source parameters.

We describe below the seismicity of Makran and focal solutions for a number of events. Focal solutions determined in this study as well as several solutions from previous studies are shown in relation to seismicity and topography in Figure 3; their focal parameters are summarized in Tables 1 and 2. We

TABLE 1. Source Parameters of Makran Earthquakes Determined in This Study

Date	Origin Time, UT	Latitude °N	Longitude °E	Depth km	M_w	m_b	Strike,[a] deg	Dip,[a] deg	Rake,[a] deg	Moment, 10^{17} N m
			Solutions From Body Waveform Inversions							
Nov. 27, 1945	2156:55.2	25.15	63.48	27	7.9		246	7	89	10200.00[b]
Aug. 5, 1947	1424:13.7	25.04	63.49	20	6.8		236	7	68	226.00
Jan. 10, 1979	0126:04.4	26.55	60.95	3	5.8		256	61	13	5.98
Jan. 10, 1979	1505:43.5	26.48	61.02	2	5.9		230	82	-4	8.80
Aug. 8, 1972	1909:31.5	25.14	61.22	18	5.0		334	15	148	0.39
			Solutions From First Motions of P Waves							
Sept. 1, 1962	1500:58.0	25.60	65.22	18		5.3	251	10	80	
Aug. 3, 1968	1401:40.7	25.19	62.87	26		4.7	290	49	-50	
Feb. 13, 1969	1111:25.3	24.99	62.75	18		5.1	279	9	84	
Aug. 6, 1972	0112:50.5	25.04	61.22	20		5.4	321	17	134	
Aug. 8, 1972	1909:31.5	25.14	61.22	18		5.4	334	15	148	
Aug. 18, 1972	1003:05.2	24.83	63.14	20		4.6	277	9	84	
Sept. 2, 1973	0723:16.6	24.88	63.21	18		5.2	281	23	70	
July 29, 1975	1325:21.0	25.22	63.09	18		5.0	278	27	88	
Feb. 10, 1978	2050:47.6	25.33	62.40	18		5.1	214	16	19	
April 28, 1980	0704:40.6	27.54	64.50	60		5.3	357	20	-172	

Latitude and longitude from ISS except for the 1945 and 1947 events for which we use locations of *Quittmeyer and Jacob* [1979]; depths are those determined in this paper, m_b from ISS.

[a] Source parameters given following convention of *Aki and Richards* [1980, p. 106]. We specify the nodal plane that we infer to be the fault plane based on its preferred orientation relative to local tectonics.

[b] Our mantle Rayleigh wave analysis yields a more reliable moment of 1.8×10^{21} N m.

TABLE 2. Source Parameters of Makran Earthquakes From Previous Studies

Date	Origin Time, UT	Latitude, °N	Longitude, °E	Depth, km	m_b	Strike,[a] deg	Dip,[a] deg	Rake,[a] deg	References[b]
May 29, 1963	0835:01.0	27.00	59.40	52	5.2	46	18	-90	C (F)[c]
						195	82	187	C (F)
Aug. 12, 1963	1829:39.7	25.32	63.14	5	5.4	190	30	0	Q (S)[c]
Aug. 2, 1968	1330:23.3	27.54	60.92	62	5.7	118	16	-60	JM (F)
				65	5.7	57	22	-116	JQ (F)[c]
				62	5.7	183	29	32	N (F)
Nov. 7, 1969	1834:04.3	27.80	60.02	35	6.1	18	30	-16	JM (F)
				74	6.1	25	26	-161	JQ (F)[c]
				35	6.1	360	37	180	N (F)
Aug. 6, 1972	0112:50.5	25.04	61.22	33	5.5	292	22	114	C (F)
				30	5.4	231	41	49	Q (S)
				33	5.5	292	20	90	JM (F)
Aug. 8, 1972	1909:31.5	25.14	61.22	30	5.5	280	5	90	C (F)
				41	5.4	223	18	34	Q (S)
				41	5.5	292	20	90	JM (F)
Nov. 17, 1972	0909:01.7	27.40	59.14	65	5.4	102	15	-90	C (F)
						163	32	20	C (F)
				65	5.4	159	80	20	JM (F)[c]
Sept. 2, 1973	0723:16.6	24.88	63.21	30	5.3	270	30	90	Q (S)
Jan. 10, 1979	0126:04.4	26.55	60.95	33	5.9	300	40	90	JM (F)
Jan. 10, 1979	1505:43.5	26.48	61.02	33	5.9	300	34	90	JM (F)
April 28, 1980	0704:40.6	27.54	64.50	34	5.4	90	6	-90	JM (F)
April 18, 1983	1058:51.2	27.79	62.05	65	6.5	83	32	-67	L (B)[c]
			Representative Solutions From Fault Zones Bounding Makran						
Dec. 10, 1977	0546:22.5	27.50	56.74	15	5.1	248	9	78	CMT
May 6, 1978	1116:06.0	29.80	66.20	33	5.4	11	89	-11	CMT
Dec. 10, 1978	0130:16.3	28.59	66.06	33	4.8	179	86	-12	CMT
Feb. 7, 1983	1506:26.6	26.28	57.21	33	5.5	5	42	172	CMT
Oct. 2, 1984	0319:40.7	26.96	66.45	13	5.2	191	76	0	CMT

[a] Source parameters as in Table 1.

[b] References: C, *Chandra* [1984]; CMT, centroid moment tensor, e.g., *Dziewonski et al.*[1983]; JM, *Jackson and McKenzie* [1984]; JQ, *Jacob and Quittmeyer* [1979]; L, *Laane and Chen* [1989]; N, *Nowroosi* [1972]; and Q, *Quittmeyer and Kafka* [1984]. Data type: F, first motion of *P* waves; S, surface wave analysis; B, body waveform inversion.

[c] Solution shown in Figures 3, 4, and 5.

focus in particular on the great earthquake of 1945 because its moment constitutes approximately 95% of the seismic moment release along Makran during this century and because its source parameters have remained unknown prior to this study.

Seismicity of Makran

The southern plate boundary of Eurasia (Figures 1 and 2) is marked by a high level of seismicity along the broad Zagros fold-and-thrust belt to the west of Makran and along the north striking transpressional zone in Pakistan to the east of Makran. In contrast, a lower level of seismicity occurs along the Makran portion of the Eurasian plate boundary. Not only is the level of seismicity in Makran low for this plate boundary, it is low in comparison to most other active subduction zones. The impingement of the Arabian (or Musandam) Peninsula of Oman on the Iranian shelf dominates the tectonics of the eastern Zagros [*Kadinsky-Cade and Barazangi*, 1982]. The Arabian Peninsula extends beneath the Straits of Hormuz as a large basement ridge [*White and Ross*, 1979] and underthrusts the continental crust of Iran. Nearly all of the seismicity associated with this collision occurs at depths less than 20 km [*Jackson and McKenzie*, 1984]. The transition from that collision to the subduction of oceanic crust in western Makran is marked by a sharp contrast in seismicity near 57.5°E (Figure 1). Another change in seismicity is associated with the eastern boundary of Makran.

Within the Makran zone itself the level of seismicity varies appreciably. In western Makran a broad aseismic region extends arcward from the deformation front for nearly 200 km (Figures 1, 3, and 4). A high-gain array of ocean bottom seismometers placed offshore of western Makran detected no microearthquakes in that region [*Niazi et al.*, 1980]. Figure 1 shows seismic events extending eastward from the Zagros to central Makran before turning south to join the coastal seismicity of eastern Makran. Most of the inland events in western Makran occur at intermediate depths within the downgoing plate and hence are not continuous with the shallow earthquakes of the Zagros. Reflection and refraction data show that the Arabian plate is currently underthrusting the accretionary wedge of western Makran along an active deformation front near the 3000-m contour [*White*, 1982; *White and Louden*, 1982]. Thus the main plate boundary between Arabia and Eurasia appears to follow the Minab fault system as far south as the deformation front of westernmost Makran and then to extend easterly along the deformation front into eastern Makran (Figure 2).

Across the NNW trending mountains that follow the Sistan suture zone (Figure 2 and 3) the seismicity pattern changes completely. These mountains include the largest Quaternary volcanic edifice, the Taftan, with the highest elevations in Makran (4100 m). The range extends NNW nearly 1100 km. Weak seismicity is found along most of this mountain range. A cluster of events at 26.5°N in 1979 produced several moderate-sized earthquakes. These events lie within the upper plate and show right-lateral motion between the Lut and Helmand blocks. The interiors of these blocks experience little seismicity. The seismic activity suggests that the Sistan suture continues to be an active tectonic zone and probably plays a role in the segmentation between eastern and western Makran. Nevertheless, while some plate motion may be accommodated along the Sistan suture and to the north of western Makran, we conclude that significant plate motion is associated with subduction at the deformation front of western Makran as it is in eastern Makran.

In eastern Makran, seismicity forms a relatively narrow, east-west band near the coast. Most of these earthquakes are of small magnitude. The epicenters of all well-documented large (M_w > 7.0) or great earthquakes of Makran also fall within this band of seismicity (Figure 6). These coastal earthquakes delimit the

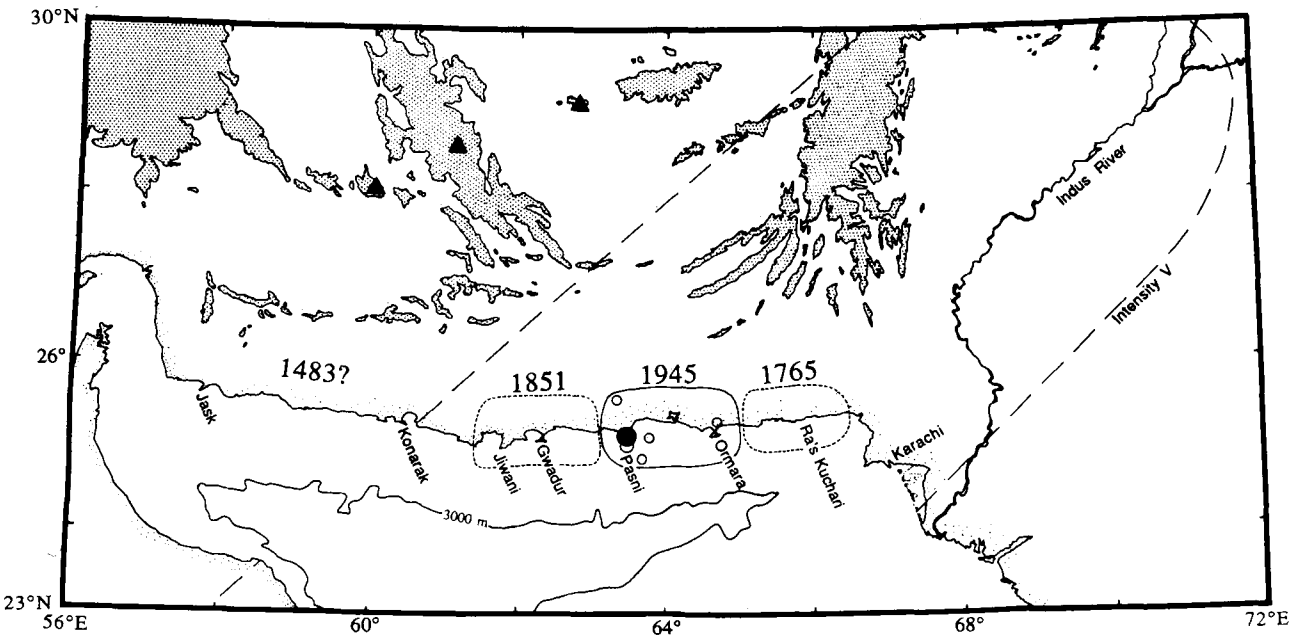

Fig. 6. Historical great earthquakes of Makran. Maximum estimated rupture areas are shown for historic sequences; thin solid line shows our estimate of the approximate rupture area of the 1945 earthquake (see text for discussion). The epicenter of 1945 mainshock is shown as large solid circle; aftershocks shown by open circles. The intensity 5 isoseismal of 1945 event from *Pendse* [1948] is shown as long dashed line. Solid triangles mark major volcanic centers. Regions elevated more than 1500 m are enclosed by dotted pattern.

most seaward seismic slip along the plate boundary, thereby defining the seismic front for Makran (Figure 5), i.e., the seaward limit of seismicity along the plate boundary. The seismic front indicates that point at which motion along the plate boundary changes from largely seismic slip within well-consolidated rock to aseismic slip within unconsolidated sediments near the deformation front [*Byrne et al.*, 1988]. The aseismic zone in eastern Makran extends seaward from the seismic front approximately 70-80 km out to the deformation front.

Across northern Makran a number of intermediate-depth earthquakes form an ENE trend about 400-500 km from the deformation front. These events make up much of the seismicity seen in the west, and although fewer in number, they continue across eastern Makran. These few events occur within the downgoing plate and include a number of larger earthquakes that have normal faulting focal mechanisms [e.g., *Jackson and McKenzie*, 1984; *Laane and Chen*, 1989]. These events have predominantly downdip T axes, indicating that the subducted slab is in tension.

Historical Record of Large Earthquakes

The desert coast of Makran has remained a remote region from the early Islamic period (600 A.D.) through the seventeenth and eighteenth centuries, leading to an historic record of earthquakes that is short relative to the long span of adjacent civilizations to the east and west [*Ambraseys and Melville*, 1982]. The first submarine cable along the Makran margin was laid in 1864, and the coastal towns were connected to the telegraph network during the first world war. Even today the communities along the coast remain small, and a still smaller population is found inland. We have some reports of great earthquakes dating back over 500 years. However, the record is certainly not complete over that length of time. The historic record appears to be complete for large ($M_S \geq 7.0$) earthquakes since the mid-nineteenth century and probably for much longer for great ($M_S > 7.7$) events, particularly near the eastern and western boundaries of Makran [*Ambraseys and Melville*, 1982].

The historic record places seven large earthquakes in Makran. Six of these shocks may have ruptured the plate boundary in four different segments (Figure 6). The other large event occurred in 1914 in northern Makran [*Gutenberg and Richter*, 1954]. Gutenburg and Richter reported that this event occurred at a depth of 60-100 km indicating that it was within the downgoing plate. Its location in northern Makran where other intermediate-depth events occur adds credence to their depth estimate.

An earthquake in 1483 affected the Strait of Hormuz and northeast Oman and may therefore have occurred somewhere in western Makran, but a more specific location is not possible. It might have occurred in the eastern Zagros. This is the only known earthquake that may potentially have struck western Makran. Another event in 1765 was felt strongly at Ra's Kuchari in easternmost Makran. Two coastal events occurred in 1851 and 1864 affecting the town of Gwadar [*Quittmeyer and Jacob*, 1979; *Oldham*, 1882], again in eastern Makran. In 1945 a great earthquake struck the coast of eastern Makran near Pasni, followed by a large aftershock in 1947 immediately to the south. The maximum area along the plate boundary (projected to the surface) that may have ruptured during each of these historic sequences are shown in Figure 6. The rupture zones of the 1851 and 1765 shocks could well have been smaller than that shown, as these areas are not well constrained. In Figure 6 we have considered the 1864 event to have occurred within the 1851 rupture area because they affected the same towns. We centered the rupture areas on the region affected by each event and outlined abutting ruptures areas with sizes appropriate for events of approximately magnitude 8. The rupture area of the 1945 event is better constrained, as discussed below. The source mechanism of the 1945 event is the subject of a detailed study described in the next section. Two important observations drawn from the historic record are that large and great earthquakes occur at Makran, and that the distribution of historic events is highly asymmetric with most (and perhaps all) of the activity being confined to eastern Makran. Whether any of the plate boundary in western Makran has ruptured in a large or great earthquake during the last 600 years is questionable. Whether most or all of the plate boundary in eastern Makran broke in the three shocks shown in Figure 6 is also questionable.

THE GREAT EARTHQUAKE OF 1945

The initiation of rupture in the great earthquake of November 27, 1945, 2156:55.2 UT (universal time), occurred at 25.15°N 63.48°E [*Quittmeyer and Jacob*, 1979], placing the epicenter just offshore from the town of Pasni (Figures 5 and 6). The depth of the event has not been analyzed before this study. The accuracy of the hypocentral location appears to be poor, especially by present-day standards; we do not consider it to be a tight constraint on the location of rupture along the plate boundary. In Figure 5 we show the hypocenter (large circle beneath the plate boundary) determined by *Quittmeyer and Jacob* [1979] as well as our interpretation of the region that actually slipped during this event (striped section of the plate boundary). The estimated rupture area is based on our body wave analysis and dislocation modeling rather than the hypocentral location. A number of authors have assumed a thrust faulting focal mechanism for the 1945 event because of its location at a subduction zone and its large magnitude [e.g., *Jacob and Quittmeyer*, 1979; *Page et al.*, 1979]. *Laane and Chen* [1989] recently concluded, however, that the first motions of P waves are inconsistent with thrust faulting, leading them to propose a normal faulting focal solution instead. Our initial study of this event based largely on first motions of P waves, S wave polarizations, and surface wave amplitude ratios led us to the same conclusion [*Byrne et al.*, 1989]. Analysis of body waveforms for the 1945 event and its large aftershock of 1947 and dislocation modeling of coastal uplift, however, shows that these events are unquestionably thrust earthquakes, presumably occurring along the plate boundary. Body waveform inversions of P and SH waves provide the most definitive results. In this section we describe those data as well as all additional data including first motion of P waves, surface waves, and dislocation modeling of the coastal uplift.

Tsunami, Mud Volcano Activity, and Intensities of 1945 Earthquake

The 1945 event caused widespread damage along the very sparsely populated coast and generated a large tsunami. Tsunami heights are estimated at 5-10 m along the coast adjacent to the epicenter at Pasni and Ormara [*Pendse*, 1948; *Ambraseys and Melville*, 1982]. The initial wave shortly after the event did not come far inland; the destructive tsunami that

swept over the town of Pasni reportedly occurred 90-120 min after the earthquake [*Ambraseys and Melville*, 1982] (3 hours according to *Pendse* [1948]). The long delay of the tsunami following the main shock appears well documented in these references but remains unexplained. The tsunami was 1.5 m high at Karachi (360 km distant), 2 m near Bombay (1100 km away), 0.5 m in the Seychelles (3400 km away), and caused noticeable effects at Karwar (1500 km distant) and at Muscat [*Pendse*, 1948; *Ambraseys and Melville*, 1982]. The transoceanic cable between India and England broke in eight places, indicating widespread slumping offshore. Part of the town of Pasni moved with one submarine slide shifting the coast 100 m landward. The event caused intense mud volcano activity resulting in the creation of four new mud volcano islands (Figure 2) 8-30 m in height in water 7-13 m deep [*Sondhi*, 1947], extensive venting of mud and gas along the coast, and the reactivation of the mud volcanoes near Hinglaj (approximately 35 km WNW of Ra's Kuchari, Figure 6) where a large volume of natural gas escaped and ignited. At Ormara a sudden elevation of the water table caused flooding [*Ambraseys and Melville*, 1982]. Coastal uplift associated with this earthquake was best displayed at the Ormara tombolo that permanently raised 2 m [*Ambraseys and Melville*, 1982; *Page et al.*, 1979]. Unfortunately, no uplift data are available away from the shoreline in either the landward or seaward direction.

The isoseismals of the 1945 event as determined by *Pendse* [1948] are very asymmetric with much greater intensities extending toward the northeast (Figure 6). That direction is parallel to the dominant structural trend in eastern Makran (Figure 2), the Indus River valley, as well as the largest concentration of population. The asymmetry of the isoseismals is probably related to these factors and not to the rupture parameters per se. In Gwadar the event caused only slight damage and was not felt strongly west of Jiwani, only 95 km west of Pasni [*Ambraseys and Melville*, 1982]. Yet toward the east and northeast of Pasni greater intensities and damage were noted. These observations suggest that most of the rupture area lies east of Pasni. The distribution of the associated mud volcano activity and the large uplift at Ormara support that interpretation. The number of aftershocks associated with this event appears to be quite low according to the International Seismological Summary (ISS). Only five events over the next five years were of sufficient size to be reliably located (Figure 6). One of these earthquakes is the large event of 1947 that was located immediately to the south of the mainshock. The remaining four events were not recorded by enough stations to be jointly relocated [*Quittmeyer and Jacob*, 1979]. The limited aftershock data also suggest that the rupture extended dominantly to the east (Figure 6).

Determination of Source Parameters for 1945 and 1947 Earthquakes

We used body waveform modeling, first motion of *P* waves, *S* wave polarizations and surface waves to determine the focal mechanism, depth, and moment of the 1945 earthquake and its aftershock of 1947. We obtained 34 seismograms from 19 stations for the 1945 event and 20 seismograms from 12 stations for the 1947 aftershock. It should be remembered, however, that the 1945 event occurred shortly after the end of World War II when many seismograph stations were not operating. Thus the available seismic data are relatively poor compared with more modern data. Nevertheless, a sufficient number of these records were useful for one or more aspects of our study, and the data allow us to constrain the source parameters.

Waveform inversion of P and SH waves. We employed the technique of *Nábělek* [1984] to simultaneously invert long-period *P* and *SH* waveforms for source mechanism, centroid depth, scalar seismic moment, and the far-field source time function. The inversion technique uses a point source parameterization given by equal time segments each with arbitrary moment; for larger events we use a line source that assumes fault segments of equal length (each with arbitrary moment) that rupture at a prescribed velocity [*Nábělek*, 1984, 1985]. The latter parameterization allows the effects of source finiteness (extended rupture area) and rupture propagation to be included in the synthetics. The inversion procedure then minimizes the difference between the observed and synthetic seismograms in a least squares sense to determine source parameters. We assumed a double-couple mechanism throughout our analysis. Results of the inversions are summarized in Table 1.

In the inversions discussed in this paper we restrict the distance range for *P* waves to lie between 30° and 90° and for *SH* to 30° to 80°, thereby minimizing the effects of upper mantle discontinuities associated with shorter distances and of the core at larger distances. Few historic seismograms proved useful for the inversion procedure; most of the records within this distance range were either off-scale or too small or had other shortcomings. For the 1945 event vertical component *P* waves were well recorded by the Galitzin seismograph at DeBilt and by the 1-60 s Benioff galvonometer system at Weston. Weston lies just beyond our distance limit (101°), but given the limited data available, we include it in the inversion. Some *P* wave energy loss occurs as diffraction around the core in reaching Weston so that the seismic moment derived from this record will be underestimated. We determine the moment independently and more reliably, however, using Rayleigh waves as described below. The horizontal Galitzins at DeBilt provide the only useful source of shear wave data. The *S* wave was well recorded at Uppsala as well, but the single inverted pendulum of the Wiechert seismometer exhibited coupling between the horizontal records making the rotation required to produce an *SH* wave dubious [*Kanamori*, 1988]. More seismograms remained on-scale for the 1947 event. This smaller-magnitude (M_S 7.3) event generated simpler waveforms. We obtained four useful *P* wave seismograms (Sverdlovsk, DeBilt, Copenhagen, and Weston) and four *SH* waveforms (Sverdlovsk, Kew, DeBilt, and Copenhagen). We hand-digitized the available records, removed the effects of pen-arm curvature when necessary, and interpolated the seismograms to 1 sample per second. The instrument constants we used in calculating synthetics for these stations are listed in Table 3. The crustal velocity model employed for the source region (Table 4) is based on marine refraction studies near the Makran coast [*Niazi et al.*, 1980; *White and Louden*, 1982]. It includes a large thickness of low velocity sediments capped by a thin water layer.

We began our inversion procedure with the 1947 earthquake because its waveforms are simpler than those of the mainshock. Figure 7 shows the observed and synthetic seismograms from this inversion. A simple, triangular source time function of 14 s duration adequately matched the waveforms. Significantly better fits were not provided by more complex source parameterizations. Our preferred solution

TABLE 3. Instrumental Constants

Station	Comp	Instrument	Natural Period, s		μ [a]	l	A_1	k	$A_1 k/\pi l$
			Ts	Tg			mm		
Copenhagen	Z	Galitzin-Wilip	10.8	11.6	0.00	144	1000	105	232.1
	N	Galitzin-Wilip	12.3	12.6	0.14	125	1000	100	254.6
	E	Galitzin-Wilip	12.3	12.6	0.14	125	1000	107	272.5
De Bilt	Z	Galitzin	12.0	12.0	0.00	406	1380	175	189.3
	N	Galitzin	25.0	25.0	0.00	123	1380	11	39.3
	E	Galitzin	25.0	25.0	0.00	123	1380	11	39.3
Kew	N	Galitzin	8.2	24.5	0.00				74.3
	E	Galitzin	8.0	24.0	0.00				81.5
La Paz	Z	Galitzin	10.0	11.8	-0.09	148	1255	128	345.5
Sverdlovsk	Z	Galitzin	12.7	12.8	0.03	399	1459	476	554.0
	N	Galitzin	25.2	24.8	0.06	124	1323	53	180.0
	E	Galitzin	25.0	25.0	-0.09	124	1336	47	161.2
Wellington	Z	Galitzin-Wilip	5.0	10.6	-0.03	14	112	155	394.7

Station	Comp	Instrument	Natural Period, s		Damping		Magnif-ication
			Ts	Tg	Ds	Dg	
Pasadena	Z	Benioff	1.0	90.0	0.0	0.0	1500
Weston	Z	Benioff	1.0	60.0	0.7	0.0	3000

[a] Parameters obtained from individual stations with the seismograms or from *McComb and West* [1931] and *Charlier and van Gils* [1953]. See *Sohon* [1932] for details about Galitzin instrumental parameters.

shows one nodal plane striking 236° and dipping 7° to the north and a centroid depth of 20 km. The solution is consistent with the depth and dip of the plate interface estimated from refraction data [*White and Louden*, 1982], indicating that the 1947 event involved thrust motion along the shallow dipping plate boundary.

Our inversion for the source parameters of the great 1945 earthquake commenced with the solution from the 1947 event. A point source with a thrust mechanism similar to that of the 1947 event was used to generate waveforms similar to the initial part of the 1945 waveforms. For the mainshock, however, both the *P* and *SH* waves ring on with secondary pulses of larger amplitude (Figure 8). We interpreted these as representing source complexity, i.e., that the source for the 1945 event involved several subevents. Models using a point source extended in time required a duration exceeding 60 s making a point source parameterization unrealistic. The data for the mainshock therefore required that the effects of source finiteness and rupture propagation be included in the synthetics.

We inverted for the location of the center of moment release, the centroid, relative to the nucleation point. The final synthetics are shown in Figure 8. The preferred solution places the centroid 55±11 km along an azimuth of 168°±20° relative to the nucleation point. A further reduction in misfit of the synthetics is gained by adding a line source parameterization with a constant rupture velocity (which we constrained to be 1.5 km/s). Our solution suggests that rupture propagated south-southeastward. This direction is consistent with the limited aftershock distribution, the location of the 1947 epicenter just to the south of that of the 1945 event, and evidence that damage along the coast was predominantly east of the epicenter (Figure 6). The centroid depth we determined for the event is 27±3 km. The source depth is dependent upon the velocity model; the model we employed (Table 4) was extrapolated from refraction data farther offshore [*White and Louden*, 1982]. The solution places the center of moment release slightly beneath the plate boundary, suggesting that our model velocities are somewhat fast. The preferred source time function consists of three pulses growing in amplitude with a total duration of 56 s (Figure 8).

Such details of the rupture process generally cannot be uniquely determined from long-period data, even when high quality records are used with good azimuthal distribution [e.g., *Boyd and Nábělek*, 1988]. Similarly, the details of the 1945 rupture process are neither unique nor well constrained with only two *P* and one *SH* waveform. This solution, however, provides the greatest reduction in the misfit between available data and synthetics over point source and other simpler models. In addition, the solution is consistent with the locations of aftershocks, with mud volcano activity, and with damage along the coast. We are confident about several important source parameters: the 1945 event involved thrust faulting, the shallow depth indicates that rupture occurred along the plate boundary, the source included some complexity with a low amplitude onset, and rupture duration was at least 56 s, implying a rupture area with a diameter of about 80-150 km depending on the rupture velocity. We have assumed that the long dimension of the rupture was along strike (Figure 6) and that the downdip length of rupture was approximately 100 km. These latter details are not well constrained, however, and it is quite possible that the rupture area was more square-shaped or even extended a greater distance in the downdip direction. Our inferred downdip limit of rupture is, in fact, rather shallow compared to many subduction zones, so it is possible that the

TABLE 4. Crustal Structures Used in the Makran Region

Region	Thickness, km	V_p, km/s	V_s, km/s	Density, g/cm^3
Near Coast	1.0	1.5	0.0	1.0
	4.0	3.5	2.0	2.4
	12.0	4.5	2.4	2.6
	6.0	6.7	3.9	2.7
	half-space	7.9	4.6	2.8
Inland	2.0	2.9	1.7	2.1
	10.0	5.3	3.1	2.4
	12.0	5.9	3.4	2.6
	3.0	4.2	2.4	2.3
	half-space	7.9	4.6	2.8

In all cases a homogeneous half-space was used for the receiver crustal structure with $V_p = 6.5$, $V_S = 3.8$, density = 2.7 (in above units).

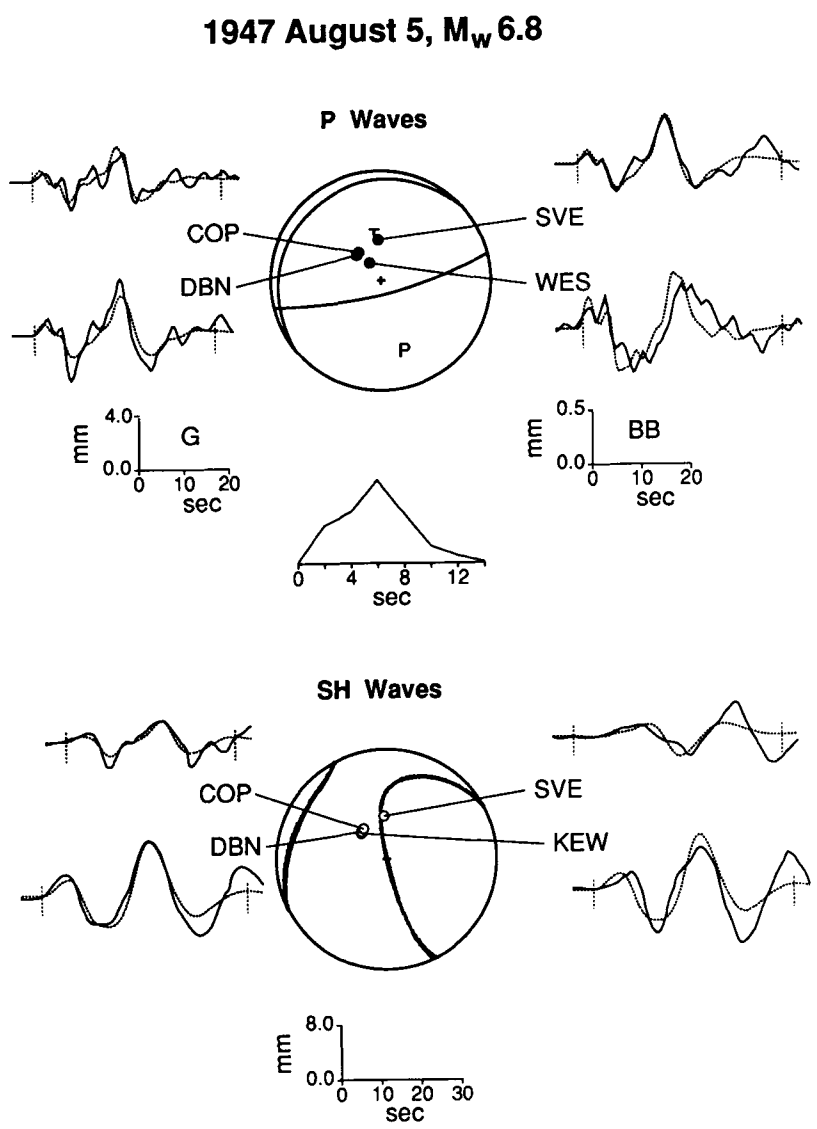

Fig. 7. Observed (solid) and synthetic (dashed) long-period seismograms for the August 5, 1947, aftershock of the great Makran earthquake. Focal solution determined from body wave inversion is shown on lower hemisphere, equal-area projections for *P* waves (top) and *SH* waves (bottom). Solid circles indicate compressional first motions. *P* wave amplitude and time scales are shown for Galitzin seismograms (G) and for broadband instrument at WES (BB); *SH* wave amplitude and time scales indicated at bottom. Far-field source time function drawn at center. All seismograms normalized to an epicentral distance of 40° and an instrument magnification of 1500.

1945 event initiated at a greater depth farther arcward and ruptured southward along a wider region in the downdip direction than we show in Figure 5. The updip limit of rupture is better constrained by dislocation models of coastal uplift as described later. We find that rupture probably did not extend more than 30 km seaward of the coast.

First motion focal solution. Ten stations showed *P* waves useful for determining first motions for the 1945 event. An additional nine *PP* wave first motions and one *PKIKP* wave were used allowing us to cover more of the focal sphere. The *PP* phase must be inverted at a range of distances to determine the equivalent *P* wave polarity [e.g., *Aki and Richards*, 1980]. First arrivals were estimated using the origin time of *Quittmeyer and Jacob* [1979], the *Herrin* [1968] travel time table, and a focal depth from our body wave inversion. Nonetheless, a number of the seismograms do not have sufficiently accurate timing to enable the onset to be precisely picked. Our first motions were combined with seven additional first motions reported in the ISS catalog to produce a first motion focal mechanism for the 1945 event (Figure 9). Table 5 summarizes the data used in this mechanism. The first motion data for the 1947 event do not allow a unique determination of a focal mechanism because most of the available polarities are from Europe and thus do not provide a good azimuthal distribution. The available first motions are consistent with those from 1945. European *S* wave polarizations from 1947 also show agreement with the 1945 solution.

The best fitting mechanism for the initiation of rupture in the 1945 shock based on first motion data indicates normal faulting [*Laane and Chen*, 1989; *Byrne et al.*, 1989] as shown by the dashed nodal lines in Figure 9. The steeply dipping nodal plane lies between the largely compressional arrivals across Europe and the USSR and the largely dilatational first motions observed near the center of the focal sphere and in the

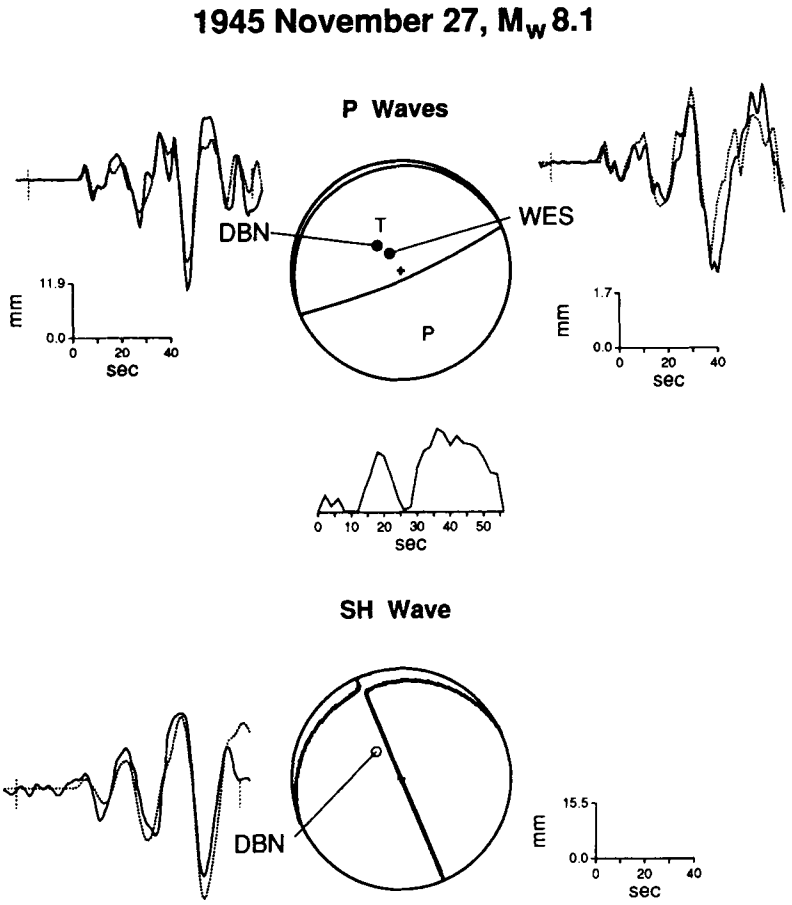

Fig. 8. Observed (solid) and synthetic (dashed) long-period seismograms for the great Makran earthquake of November 27, 1945. All symbols are as described in Figure 7. Note long source time function made up of three pulses with amplitudes increasing as a function of time.

southern hemisphere. Note, however, that four compressional data points also lie within the region of dilatational arrivals and are inconsistent with a normal faulting solution (Figure 9).

The solid nodal lines in Figure 9 indicate the focal solution derived from our body waveform inversion. This solution fits the first motion data only slightly worse than the normal solution. Furthermore, body waveform modeling strongly favors the thrust mechanism; all of our inversions for source parameters lead to thrust solutions even when the inversion was started with a normal faulting mechanism. Uplift data discussed below also suggest that the normal faulting solution is incorrect and that the 1945 event is best fit by the thrust solution. To better illustrate that the normal solution does not fit the available waveforms we have calculated synthetic *P* waves for this focal mechanism (Figure 10) and compared them to those calculated for the thrust solution. We again used the inversion technique of *Nábělek* [1984] to calculate the waveforms in Figure 10 but held the focal mechanisms fixed and used only a point source extended in time for both mechanisms. Even with this simple source the thrust solution fits the observed *P* and *SH* waveforms quite well. The normal

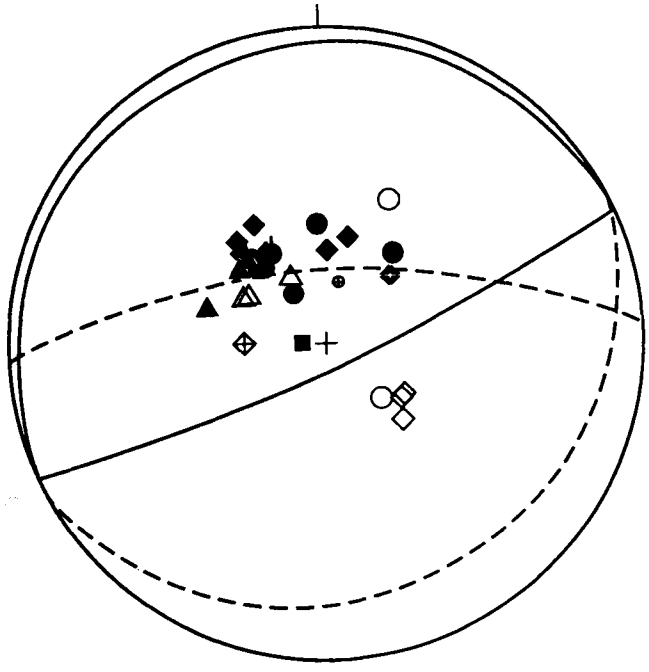

Fig. 9. Equal-area, lower hemisphere projection of body wave first motions and *S* wave polarizations for the earthquake of November 27, 1945. Circles are *P* wave first motions, diamonds are *PP*, squares are *PKIKP*, dotted line segments are *S* wave polarization angles, and triangles are polarities for *P* waves as reported by the ISS. Solid symbols indicate compressions; open symbols indicate dilatational motions. Size indicates reliability. Symbols with crosses represent questionable picks (see Figure 11 and Table 5). The focal solution that best fits the first motion data is shown by dashed lines; preferred thrust solution is indicated by solid nodal lines.

TABLE 5. First Motion Data for Earthquake of 27 November 1945

Station	Sation code	Component	Distance, deg	Azimuth, deg	Phase	Sense of Initial motion	Inferred Polarity
Pasadena	PAS	Z	121.0	1.6	*iPP*	down = dilat.[a,b]	C[c]
		N			*iPP*	up = north[a,b]	C[c]
College	COL	N	87.0	12.8	*eP*	down? = north[a,b]	D?[d]
		N			*ePP*	down = north[a,b]	C[c]
		E			*ePP*	up = west[a,b]	C[c]
Frunse	FRU	E	19.9	24.7	*iP*	down = west	D[d]
Irkutsk	IRK	E	41.0	37.8	*iP*	up = east	C
Honolulu	HON	N	118.7	44.6	*ePP*	up = north[a,b]	C[c]
		E			*ePP*	down = west[a,b]	C[c]
Wellington	WEL	Z	121.7	124.4	*iPP*	up = comp[a]	D[c]
Charters Towers	CHR	Z	120.4	127.2	*iPP*	up = comp[a]	D[c]
		N			*iPP*	down = north[a]	D[c]
		E			*iPP*	up = west[a]	D[c]
Perth	PER	N	75.7	136.0	*iP*	up = north	D
		N			*iPP*	down = south	D[c]
La Paz	LPB	Z	134.2	271.0	*PP*	up? = comp[a,b]	D?[c,d]
		Z			*iPKIKP*	up = comp	C
Kew	KEW	Z	42.9	316.5	*iP*	up = comp[a]	C
		E			*iP*	down = west[a]	C
De Bilt	DBN	Z	51.2	317.7	*iP*	up = comp	C
		N			*iP*	up = north	C
		E			*iP*	down = west	C
Edinburgh	EDI	E	56.5	321.7	*iP*	up=west[a]	C
Weston	WES	Z	100.9	327.6	*iP*	up = comp	C
		E			*eP*	down=west	C
		Z			*iPP*	down=down	C[c]
		N			*iPP*	up=north	C[c]
		E			*iPP*	up=east	C[c]
Uppsala	UPP	N	46.9	330.0	*iP*	up = north[a]	C
		E			*iP*	down = west[a]	C
		E			*iPP*	up = east[a]	C[c]
Sverdlovsk	SVE	Z	31.7	357.0	*iP*	up = comp	C
		E			*iP*	down = west	C
			Additional Polarities From ISS				
Helwan	HLW		28.8	286.6	*iP*		C
Granada	CRT		57.6	299.4	*iP*		D[d]
Lisbon	LIS		61.6	302.0	*iP*		D[d]
Belgrade	BEO		39.8	310.6	*eP*		C
Uccle	UCC		51.6	315.9	*iP*		C
Ivigtut	IVI		78.0	332.6	*P*		D[d]

[a] Sense of ground motion of component not marked on seismogram, inferred from analysis of phases or from station bulletins.

[b] Small-amplitude onset easily missed (e.g., see Figure 11).

[c] *PP* wave polarity inverted after leaving source.

[d] Motion is inconsistent with preferred solution from waveform modeling, probably incorrect pick or incorrect marking on seismogram.

synthetics, however, fail to match the initial polarity of the *P* waves and do not fit the larger amplitude pulses between 18 and 60 s.

In addition to the support for the thrust solution provided by other data sets, important shortcomings exist in the first motion data that contributed to initial interpretations of normal faulting. The small amplitude of the initial pulse of the *P* waves (as shown by the body wave inversion) contributes to the large number of incorrect dilatational polarities at the more distant stations (closer to the center of the focal sphere in Figure 9). The small initial pulse is near the noise level on a number of records allowing a larger secondary pulse to be chosen for the first arrival. Three of these dilatations are from ISS reports: Granada, Lisbon, and Ingivut. The disturbed trace in advance of *PP* waves made the choice of the first motions from these phases even more difficult. For example in Figure 11 we show two *PP* waves for which we initially chose the larger compressional arrivals that occur just to the right of the arrows as the first motion (left side, Figure 11). The interpretation of compressional *PP* phases would require that they left the source and would therefore appear on the focal sphere as dilatations. These waves are in fact more consistent with leaving the source as compressions when the correct onset is chosen: the Hilbert transform of these *PP* waveforms with a phase shift of $\pi/2$ produces *P* waves [*Choy and Richards*, 1975], and Figure 11 (right side) shows that they are quite similar to the DeBilt *P* wave. The comparison of these waveforms helps to establish the correct onset even in the presence of poor timing (arrows, right side of Figure 11). The two available *S* wave polarizations do not show strong preference for either solution.

Surface waves. We investigated the surface waves generated

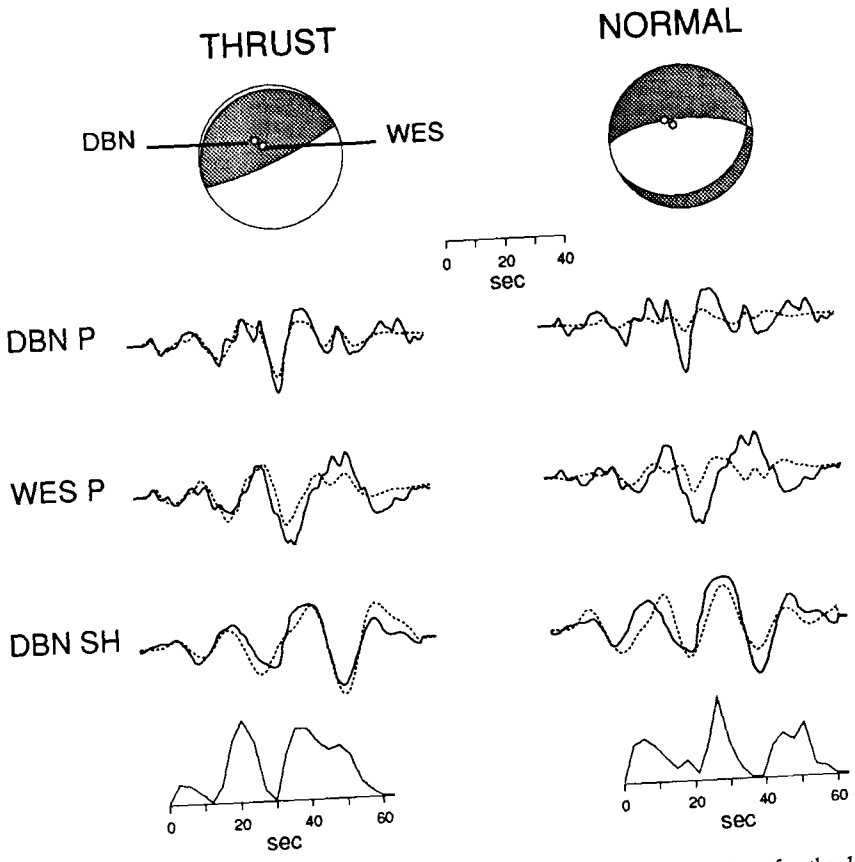

Fig. 10. Comparison of P waveforms for both thrust (left) and normal (right) faulting solutions for the 1945 earthquake. Observed seismograms are solid lines. Both sets of synthetics (dashed) are calculated with focal mechanism held fixed and a point source of 60-s duration; inversion only varied the source time function. Note that the thrust solution provides a significantly better fit; normal solution does not fit first motions nor does it match the larger amplitude pulses from 15 to 40 s.

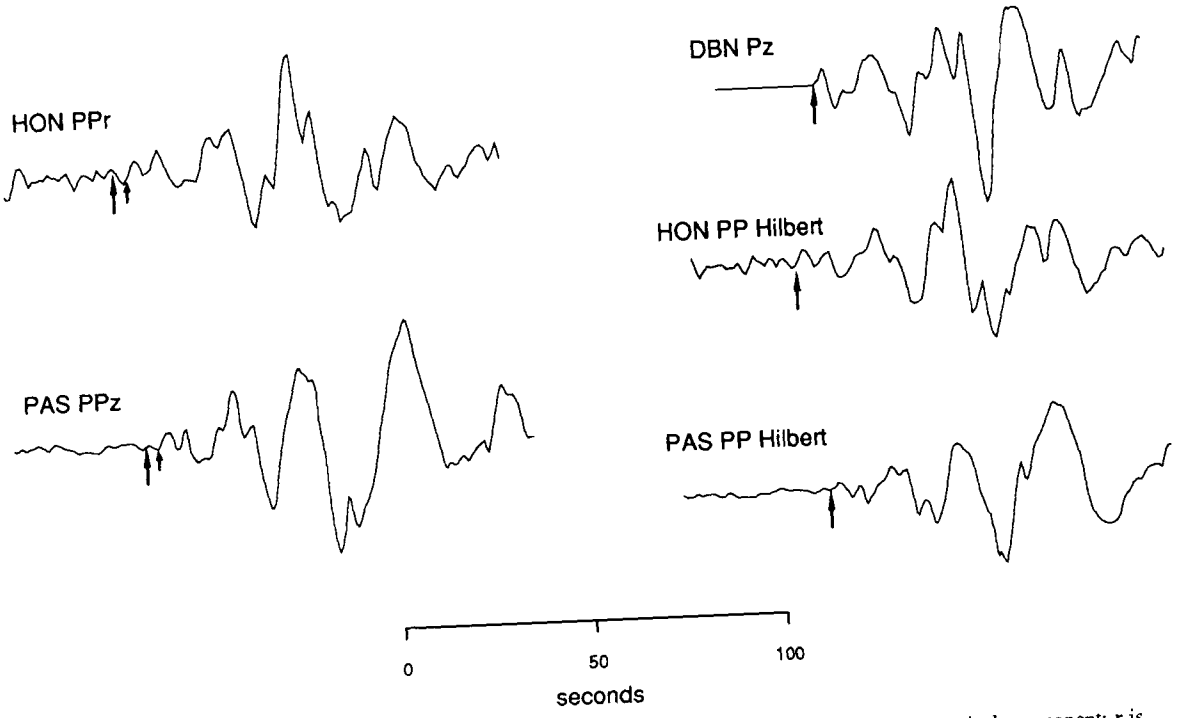

Fig. 11. Comparison of P wave at DBN and PP wave from HON and PAS for 1945 earthquake. z is vertical component; r is radial. Digitized PP waves (left) are Hilbert transformed and turned upside-down (right) to make them comparable to P waves. Note similarity in character of DBN P with transformed PP waves. For PP waves, onset is difficult to pick because of small initial source pulse (Figure 8): large arrows indicate correct onset of waves, small arrows indicate incorrect, initial choice.

by the 1945 earthquake, however, this aspect of our study was largely unsuccessful because of the poor quality of available surface wave records. Although these data did not help constrain the focal mechanism, we mention this aspect of our study for completeness. Problems we encountered with these seismograms included the large amplitude of the surface waves, which impeded our ability to follow and digitize the traces and, on some records, significant variation in the lengths of minutes and drift in timing that biased the frequency content and made rotation of surface waves impossible. In addition, for most of the available instruments we found that the signal-to-noise ratio fell below useful levels at periods greater than 75-100s thereby restricting the data to the relatively short periods that are strongly affected by lateral velocity-heterogeneity in Earth structure [e.g., *Woodhouse and Dziewonski*, 1984; *Mocquet et al.*, 1989] and further reducing the usefulness of these waves.

We attempted to use the amplitude ratios of Love to Rayleigh waves for the 1945 earthquake because amplitude ratios of different surface waves from a single station may be useful in determining source parameters from records with poorly known instrument response [e.g., *Stein et al.*, 1988]. The amplitude ratios were compared to those calculated for thrust and normal faulting mechanisms from synthetic waves generated using a normal mode summation with the code developed by Woodhouse and modified by Lerner-Lam [e.g., *Lerner-Lam and Jordan*, 1983]. Unfortunately, the two mechanisms produce quite similar amplitude ratios in the azimuths where data were available. Thus we were not able to distinguish between these patterns with any confidence with our surface wave data.

Moment Determination From Mantle Rayleigh Waves

We determined the magnitude of the 1945 earthquake using the mantle magnitude method of *Okal and Talandier* [1989]. They derive relations that provide magnitude and moment estimates from the amplitude of the inversely dispersed branch of mantle Rayleigh waves at periods greater than 50s. A magnitude or moment is calculated at each period, and the largest value is retained. The potential problems of source finiteness and of amplitude saturation inherent in magnitudes determined at a single period are thereby avoided [*Okal*, 1989]. We obtained three useful Rayleigh waves after hand digitizing the vertical component wave train and extracting the waves of interest using a group velocity window of 3.2-3.8 km/s. We estimated moment from the Rayleigh waves at Pasadena, Wellington, and LaPaz after correcting for instrument magnification (Table 3). The magnification of historic instruments may be poorly known at some stations, but we believe that the magnifications of the three instruments we used are correct at least to within a factor of 2. Seismic moment is shown as a function of frequency in Figure 12. At periods greater than 150s (0.0067 Hz) the analysis degrades as the instrument response and signal-to-noise ratios drop off. The preferred moment for each record is indicated in Figure 12 by horizontal line segments. We used values that appeared stable over at least a small range of frequencies rather than the absolute maxima. Pasadena gave stable values over the widest range of frequencies and is regarded as our most reliable station. We find seismic moments, M_O, of 1.8×10^{21} N m at Pasadena, 2.4×10^{21} N m at Wellington, and 1.2×10^{21} N m at LaPaz corresponding to moment magnitudes, M_W, of 8.1±.05, 8.2±.04, and 8.0±.05, respectively. The averaged values of M_O and M_W are 1.8×10^{21} N m and 8.1. *Gutenberg and Richter* [1954] and *Duda* [1965] assigned magnitudes of 8.25 and 8.3, respectively, to this event. Our magnitude determination is in better agreement with the lower value of M_S 8.0 obtained from more recent catalog revisions [*Geller and Kanamori*, 1977; *Abe*, 1981].

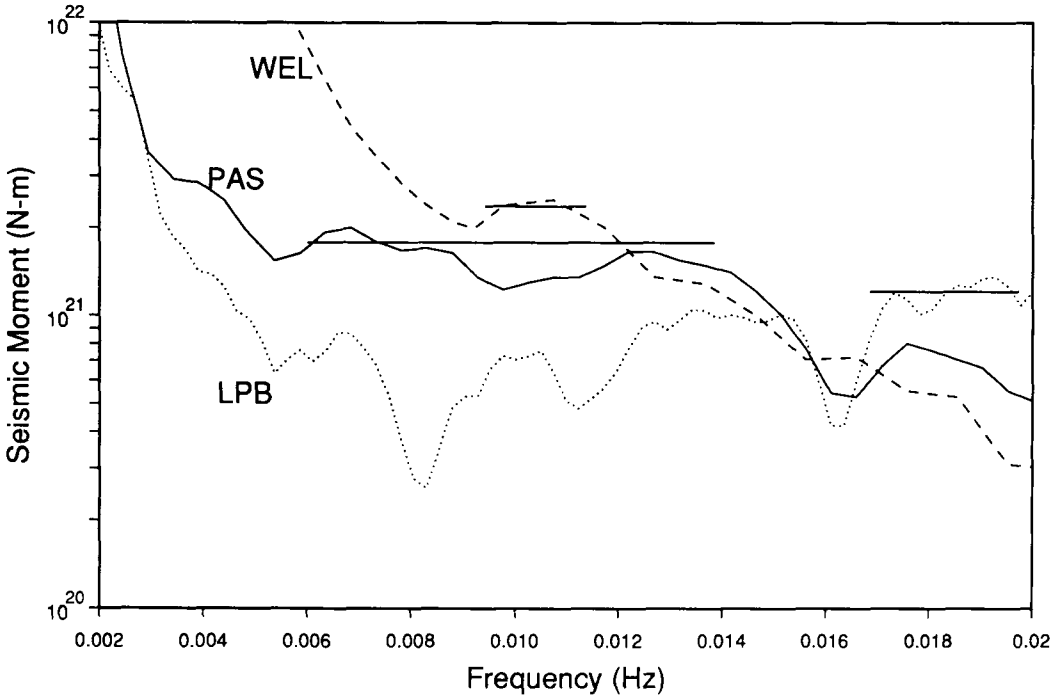

Fig. 12. Scalar seismic moment determined from vertical component Rayleigh waves at Pasadena, DeBilt, and La Paz for the 1945 earthquake plotted as a function of frequency. Moment is derived from Rayleigh wave amplitude using relation of *Okal and Talandier* [1989] (see text). Our estimates of moment for each station are indicated by horizontal line segments. At frequencies less than about 0.006 Hz (167 s) the technique degrades as the signal level drops and noise increases causing the moment values to go off scale. Note general agreement between the stations.

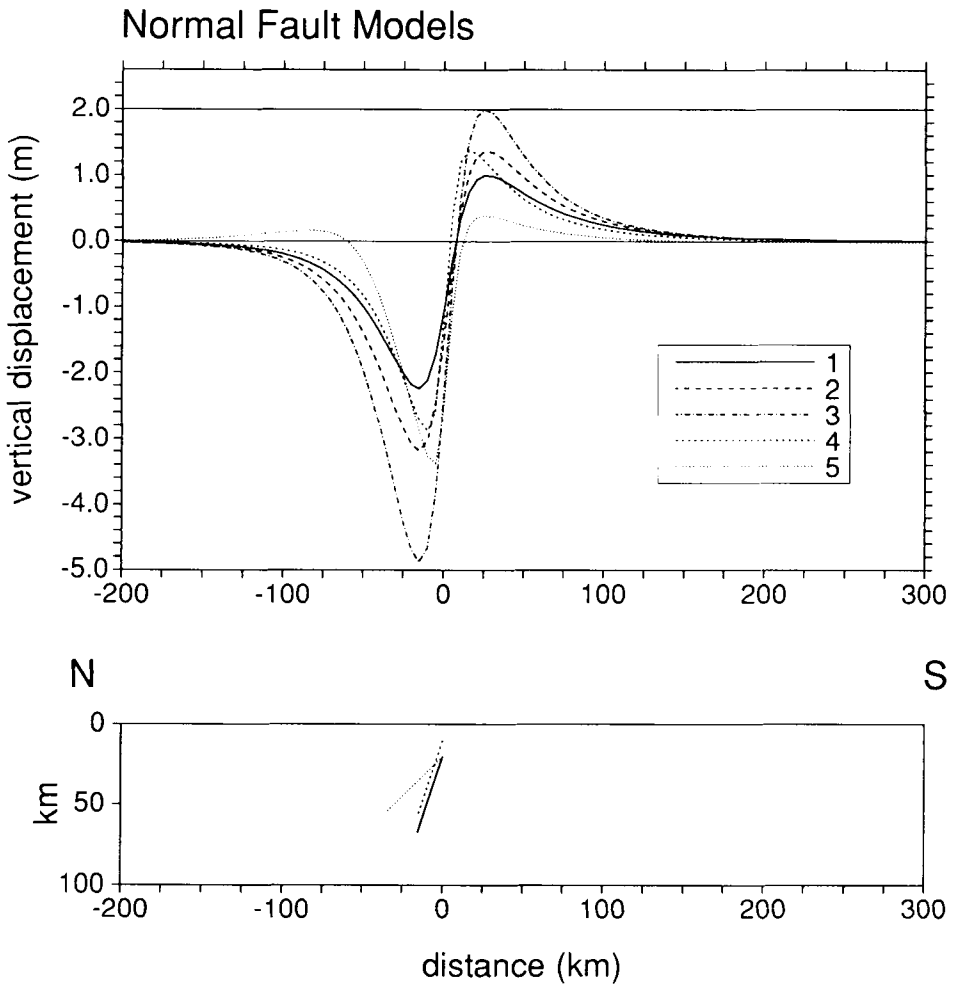

Fig. 13. Vertical displacements at the surface caused by slip on five normal-dislocation models buried in an elastic half-space. (Top) Displacements along a cross section perpendicular to strike of dislocation through its center. (Bottom) Geometry of dislocations in cross section without vertical exaggeration. Models 1, 2, and 3 overlap in bottom diagram. Distance is taken perpendicular to dislocation; 0 km marks the location of the top of each dislocation. Models 1, 2, and 3 involve displacements of 7, 12, and 16 m respectively, on a dislocation dipping 72° to the north, with a depth of 20 km to the top of the fault; model 4 has 7 m of slip and uses a fault buried less deeply; model 5 uses a fault dipping 45° with 7 m slip; note that lower dip does not increase uplift. All these models use downdip fault widths of 50 km and lengths (perpendicular to page) appropriate to produce a seismic moment of 1.8×10^{21} N m. Note that an enormous slip of 16 m is required to reach an uplift of 2 m; most of these models fail to reach that value.

Coastal Uplift and Dislocation Modeling of Rupture in the 1945 Earthquake

We employed a simple dislocation model to calculate vertical displacements at the surface produced by various faulting models and compared these with the uplift reported for the 1945 earthquake. Dislocation modeling cannot define a unique rupture model, but it places constraints on the rupture extent, magnitude of coseismic slip and the source mechanism. As noted earlier, 2 m of uplift occurred along the coast during the 1945 earthquake [e.g., *Page et al.*, 1979]. No additional uplift data exist farther inland or at sea. Additional constraints for dislocation models are provided by our body wave modeling and moment determination, the generation of a tsunami of 5-10 m near the source, and the distribution of damage and intensities along the coast. In addition, refraction and reflection data [*White and Louden*, 1982] and the location of more recent earthquakes constrain the dip and depth of the décollement that the 1945 event ruptured.

We used a buried dislocation within an elastic half space and calculated the displacements produced with models of variable fault dip, depth, rupture dimensions, slip direction, and slip magnitude. In all cases we used constant elastic properties and a seismic moment of 1.8×10^{21} N m. We scaled fault dimensions and average slip using the relation that moment is proportional to their product. We calculated vertical displacements as a function of distance for faulting models with normal faulting, thrust faulting along the plate boundary, and thrust faulting with an imbricate fault breaking the upper plate (Figures 13, 14, and 15, respectively). In all cases, 0 km corresponds to the point directly above the shallow end of the fault.

Displacements are shown for five different normal fault geometries (Figure 13) with orientations similar to the steeply dipping, dashed nodal plane of Figure 9. The calculated displacements illustrate the difficulty of generating uplift with normal faulting. These models used slips of 7, 10, and 16 m, as well as varied dips and depths. The only model that produces 2

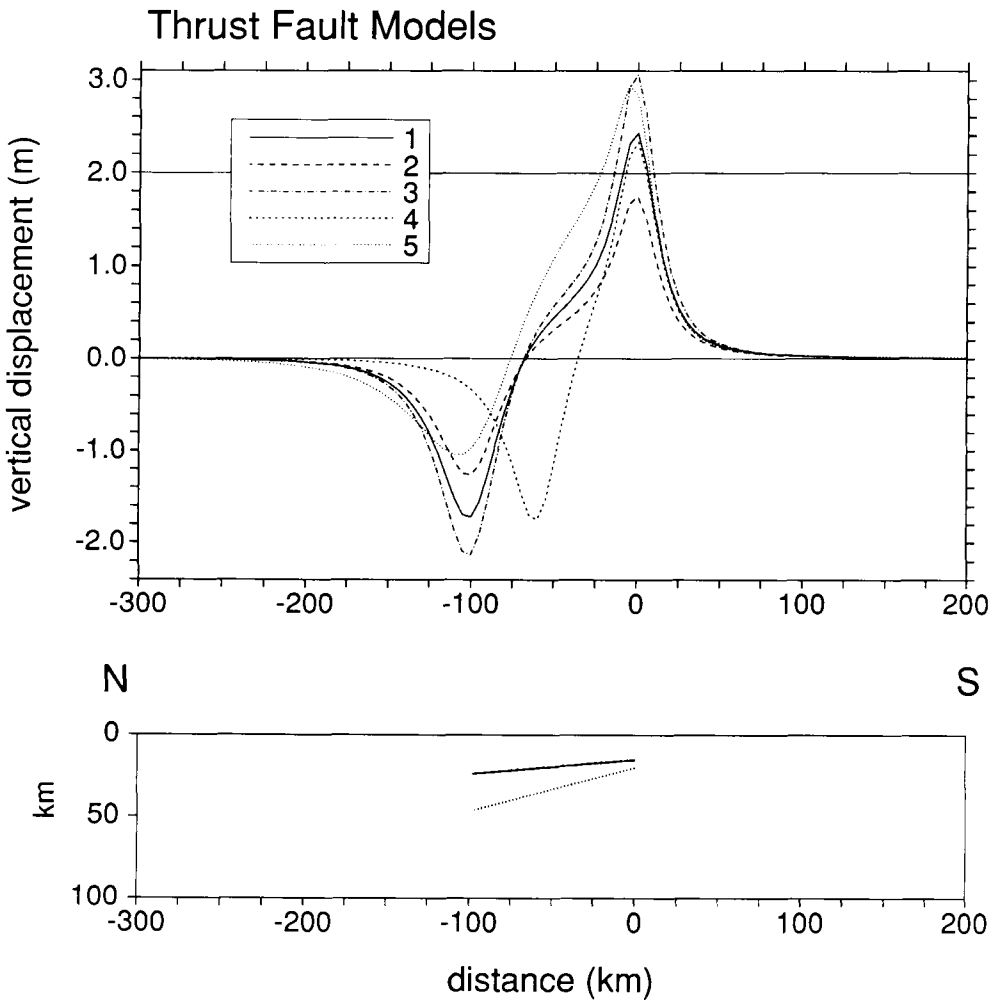

Fig. 14. Vertical displacements as in Figure 13, but for thrust dislocation models. Models 1, 2, and 3 show fault displacements of 7, 5, and 9 m, respectively, on a fault dipping 5° to the north, with a depth of 15 km to the top of the fault and a downdip width of 100 km; model 4 has 7 m of slip on a fault 75 km wide. Models 1 - 4 overlap in the bottom diagram. Model 5 has 7 m of slip on a 100 km fault dipping 15° to the north. Most of these models easily cause 2 m of uplift, but note the narrow width of the region exceeding 2 m uplift.

m of uplift required 16 m of slip along the fault, a value that is unrealistically large for an event of this size. A more shallowly dipping normal fault does not increase the uplift (compare models 1 and 5). Thus the dislocation model indicates that normal faulting could not have generated the observed surface displacements.

The vertical displacements produced by simple thrust dislocations are much larger (Figure 14), further supporting a thrust faulting mechanism for the 1945 earthquake. The details of thrusting are not tightly constrained by vertical motions at the coast alone, and a variety of models are able to accommodate the observed uplift. Our preferred single fault model used a fault dipping 5°N with the shallow limit of rupture at 15 km and a downdip rupture width of 100 km consistent with our body and surface wave modeling results. We varied rupture length and fault slip keeping seismic moment constant. We find that an average of 6 or more meters of slip produced the required uplift. The distance between maximum uplift and subsidence is proportional to the downdip width of the rupture (e.g., model 4 of Figure 14, has the least width). Steeper fault dips decrease the subsidence relative to the uplift (e.g., model 5 of Figure 14, with greatest dip). The plate boundary is known to dip very shallowly in the region of the 1945 earthquake (Figure 5), but the downdip width of rupture is not well known. In all of the models the uplifted region is confined to a narrow band centered over the upper limit of rupture. The uplift is more than half its maximum value over a region that is only 50-25 km wide for a range of models and generally near 30 km (Figure 14). The amplitude of uplift drops off sharply away from the shallow end of the dislocation. The narrow region of uplift for this class of models indicates that the seaward limit of rupture during the 1945 event most likely occurred within about 30 km of the coast.

Dislocation models that allow slip to occur both along the décollement and along an imbricate thrust that ruptures up through the upper plate allow a wider variety of models. All of these models also illustrate the essential result that uplift is confined to a narrow band centered about the shallow limit of rupture (Figure 15). Imbricate thrusts that extend up from the main thrust at steeper angles are commonly associated with great thrust earthquakes at subduction zones [e.g., *Plafker*, 1972; *Barrientos* and *Ward*, 1990]. A number of imbricate thrusts are observed uplifting strata near the Makran coast [*Ahmed*, 1969], suggesting that slip along an imbricate thrust

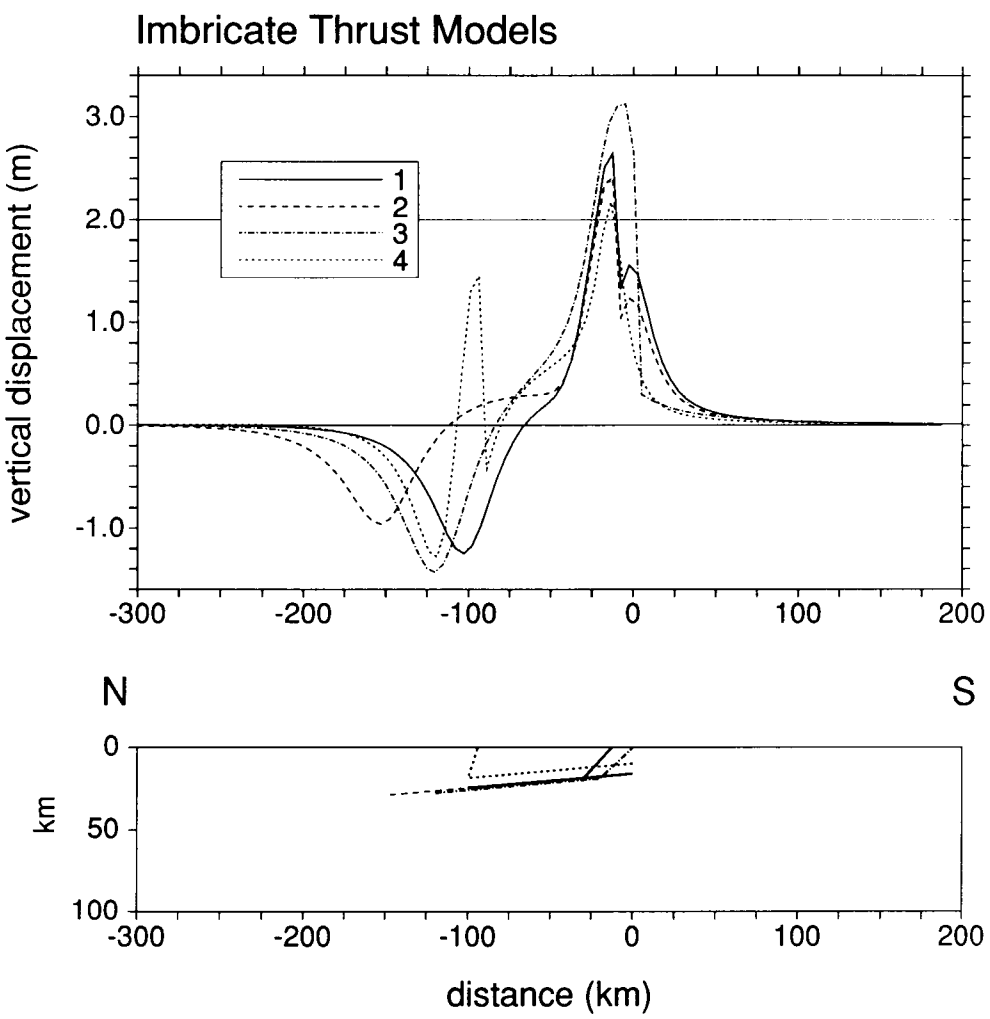

Fig. 15. Vertical displacements caused by two dislocations: a buried basal thrust and an imbricate thrust extending from it up to near the surface. 0 km marks the most southern limit of fault slip in each model. Model 1 uses a basal fault with 5 m slip, 100 km downdip width, dipping 5° to the north, and an imbricate thrust that roots into basal thrust 30 km from its top; imbricate fault has 3 m of slip and dips 42° to the north. Model 2 uses the same imbricate and basal faults as model 1 except that the basal fault extends deeper (width is 150 km) and has 3.2 m slip. In model 3, imbricate fault meets upper tip of basal thrust and displacements are 6 and 4 m on the basal and imbricate faults, respectively; basal fault is 100 km in width. Model 4 uses a shallower fault system with an imbricate fault that extends from the bottom tip of the basal thrust. Note the short distance before uplift drops off south of the limit of fault slip in all models.

associated with plate boundary rupture is reasonable. For most well-documented examples, the average slip along the imbricate thrust is a fraction of that along the main thrust [*Plafker*, 1972]. Figure 15 shows end-member models in which the imbricate fault meets the top of the ruptured segment of the décollement (model 3), the bottom of it (model 4), and the central part of it (models 1 and 2). When the imbricate fault roots into the upper part of the main fault, maximum uplift is attained because the zones of peak uplift associated with each fault add constructively (model 3 of Figure 15). When the imbricate roots at the base of the main fault, uplift associated with the former overlaps subsidence caused by the main fault and the overall uplift is reduced (model 4). In models 1 and 2 the imbricate fault joins the center of the décollement rupture area like the imbricate thrusts observed in Alaska and Chile [*Plafker*, 1972]. The uplifted region caused by an imbricate thrust is even narrower than that caused by the main thrust. One or both faults must still have an updip limit near the coast to fit the observed uplift. We find that for models with reasonable geometries the width of the uplifted region resulting from imbricate fault motion remains between approximately 15 km and 30 km (Figure 15) and the updip limit of rupture lies beneath the maximum uplift. Thus, even in the case of an imbricate fault model we find that the updip limit of rupture along the plate boundary occurs seaward of, but within approximately 30 km of, the coast.

For all the thrust models we find that vertical displacement is not very sensitive to variations in slip direction along the fault plane. The downdip extent of rupture and the dip of the fault do not strongly affect the location or amplitude of uplift. They strongly affect the relative location and amplitude of the subsidence maximum and the location of the line of zero vertical motion, but no data concerning subsidence are available. Thus the coastal uplift data alone do not constrain how far downdip rupture extended, the dip of the main fault, or the exact slip direction. We use body wave modeling and plate boundary geometry, however, to constrain the slip direction, fault strike, and dip.

We found that a simple thrust event requires an average slip of about 7 m in order to produce the observed 2 m of uplift. For reasonable aspect ratios of the rupture area and modulus of rigidity, we infer from the magnitude of the event that a maximum downdip width of rupture is approximately 100 km and the rupture length is 100-150 km. This rupture area suggests that at most one-fifth of the plate boundary at the Makran subduction zone ruptured during the 1945 earthquake. We find that even for somewhat more complex dislocation models the seaward limit of rupture is most likely no more than 30 km off the coast; simpler models place it near the shoreline. Updip rupture therefore appears to have ended near the seismic front defined by more recent seismicity (Figure 5). The plate boundary farther seaward of this at depths shallower than about 17 km did not undergo large slip or moment release in the 1945 earthquake. Thus the parts of the plate boundary that experienced co-seismic slip in 1945 and aseismic displacements at other times have similar locations to those reported by *Byrne et al.* [1988] for several other subduction zones.

FOCAL MECHANISMS OF OTHER MAKRAN EARTHQUAKES

Bodywave Inversions of Moderate-Sized Events

Most of the Makran earthquakes large enough to analyze with body wave inversion techniques occur either within the downgoing plate or along the boundary fault systems of eastern and western Makran. Only two shallow events with sufficient magnitude for body wave inversion have occurred since the installation of the WWSSN in 1963. *Jackson and McKenzie* [1984] determined thrust solutions for these earthquakes from first motion of P waves. We conclude on the basis of body wave analysis that they are strike-slip events within the upper plate.

A NNW trending zone of seismicity that extends north from the coast near 61.5°E (Figures 1 and 3) produced a swarm of events from 1978 to 1980 around 26.5°N. The largest events occurred as a pair separated by 14 hours with magnitudes of M_S 5.8 and 5.9 on January 10, 1979. We studied these events using the inversion technique of *Nábělek* [1984] as described above. We hand digitized long-period P and SH waves recorded by the WWSSN and inverted for source mechanism (strike, dip, and rake), moment, depth, and source time function. We find that both of these earthquakes occurred at very shallow depths and show strike-slip faulting with nodal planes striking northeasterly and northwesterly (Table 1 and Figures 16 and 17). These events have very similar waveforms. Both events have P waves with large second and third pulses that do not appear in the SH waves. We find that these secondary pulses are difficult to fit. They may be modeled by the use of a low-velocity zone within the source region. The similarity of waveforms for both earthquakes at the same station suggests that structure in the region near the source causes the secondary pulses because it would be unlikely to have two earthquakes with identical complex ruptures. The simplicity of the SH waves also suggest that the sources were not complex. Attempts to use complex sources including subevents with variable focal mechanisms degraded the fit of the SH waveforms and still failed to match the secondary pulses. We find that a low-velocity zone at a depth of 23 km produces a sizeable second pulse with a simple source time function. We suspect that a more accurate velocity structure is required to improve the fit to these waveforms. Previously underplated sediments accreted beneath more lithified rocks could be a source of the inferred low-velocity zone. The P axes for both events are nearly horizontal and strike SSW. The two events are part of the activity that occurs along the Sistan suture zone (Figure 2). The focal solutions are consistent with right-lateral strike-slip faulting along the Sistan suture moving the Lut block northward relative to Helmand block, suggesting that the upper plate continues to be somewhat segmented.

First Motion Focal Solutions of Small, Shallow Earthquakes

All of the earthquakes in eastern Makran in the region of the 1945 and 1947 events occurring since the installation of the WWSSN are less than magnitude m_b 5.5 and most are less than m_b 5.0. We have determined depths for a number of these events from phases reflected from the free surface and find that almost without exception they occur at or near the plate boundary (Figure 5). Such events are likely to have thrust focal mechanisms. Because of the small ($m_b < 5.5$) magnitude of these events, however, focal mechanism determination from teleseismic body wave inversion is not possible. We employed the first motions of P waves to constrain the focal mechanisms for 10 Makran events. We focused on the events near the coast, and we also determined a solution for one of the few intermediate-depth events of eastern Makran to add a constraint on the geometry of the downgoing plate. First motion solutions are difficult to constrain for events of this small magnitude. We had to rely almost entirely on short-period P waves recorded at stations with large amplification. We were aware of the large back swing following the first motion that is characteristic of short-period WWSSN instruments and took that into account in picking first motions. We employed an inversion routine (J. Pacheco, unpublished routine, 1990) to search the focal sphere and obtain the solution that both minimizes the number of incorrect polarities and places the nodal planes as far as possible from the largest amplitude arrivals and closest to the nodal arrivals. The latter decision causes the rake of the focal solution to be somewhat erratic among a group of inadequately constrained focal solutions. Our focal solutions are illustrated in Figure 18. For the events near the coast our aim was primarily to distinguish thrust from other types of events. Several of the events have limited data that do not provide a well-constrained focal mechanism (e.g., 720818, 730902, 620901 of Figure 18). Nevertheless, the broad region of compressional arrivals around the center of their focal spheres strongly suggests that they are thrust events. Obviously, the rakes for such events are not well constrained, and the variation among the thrust solutions is most likely an artifact of the limited data. We also estimate the focal depths of these events using the short-period depth phases and the velocity model (Table 4) determined from refraction studies [*White and Louden*, 1982; *Niazi et al.*, 1980].

The events from 1972 occurred as a swarm of earthquakes in central Makran near the coast. The mainshocks of this sequence occurred on August 6 and 8, both with magnitudes of m_b 5.4 (Figure 3). We have determined the first motion focal solutions for these events and find them to be thrust faulting earthquakes as did *Jackson and McKenzie* [1984] (Table 2). These events are thus the largest recent thrust events along the Makran margin. The depth of these events are found on the basis of depth phases to be 18-20 km, placing them at or near

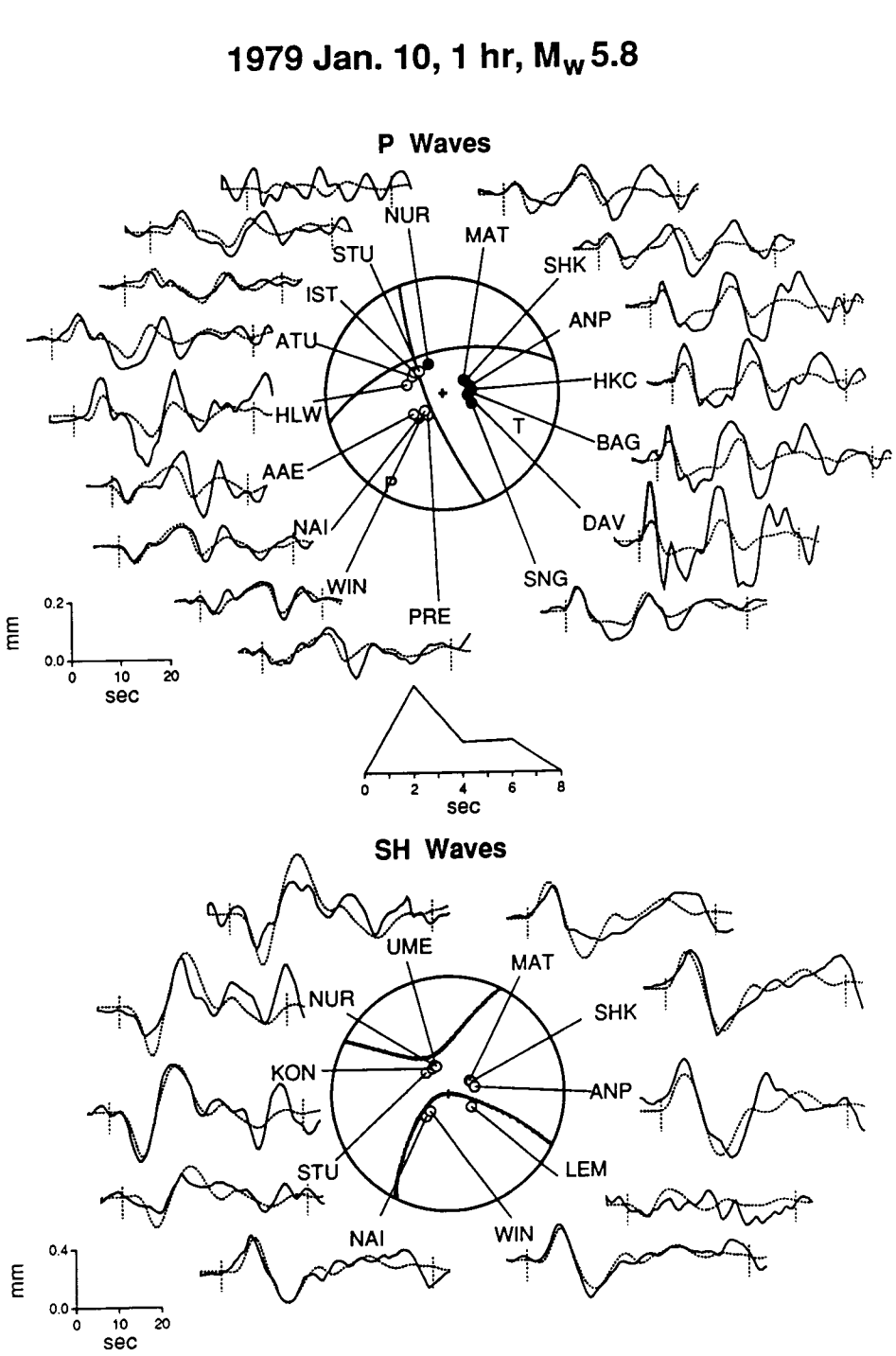

Fig. 16. Observed (solid) and synthetic (dashed) long-period seismograms for the central Makran earthquake of January 10, 1979, 1 hour. All symbols are same as Figure 7.

the plate boundary. Their long-period P waves are of insufficient amplitude at teleseismic distances for body waveform modeling. The event of 720808, however, generated short-period P waves with a high signal-to-noise ratio and we modeled these waveforms to further constrain the focal parameters following the example of and *Nábělek and Suárez* [1989]. Short-period body waves are highly dependent on the anelastic attenuation along the path from the source to the station, but this does not strongly affect the determination of focal depth or mechanism [*Nábělek and Suárez*, 1989]. For this reason, we do not place much significance on the source time function or on the moment obtained in our inversion, but we do feel confident about the focal mechanism. The depth is obviously dependent on our assumed velocity structure; we used the near-coast velocity model (Table 4). We caution that this velocity model does not contain the suspected low-velocity zone mentioned in the previous section. Thus the 18 km depth we determine, as well as those of all the events in the second part of Table 1, could be wrong by a few kilometers. Their depths relative to each other, however, would not change. We inverted the short-period waveforms for both amplitude and shape, and assumed a simple point source. Our thrust-faulting

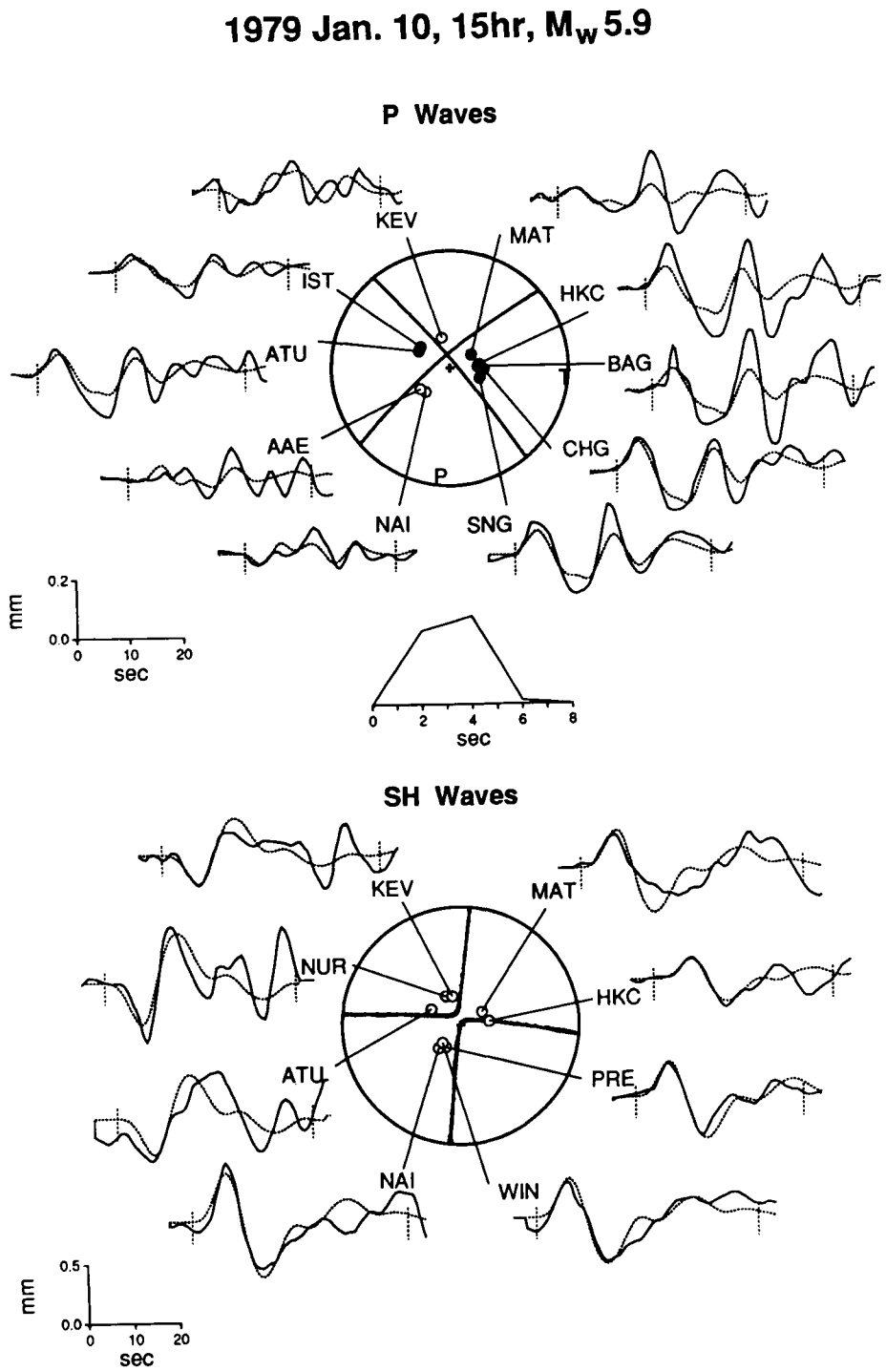

Fig. 17. Observed (solid) and synthetic (dashed) long-period seismograms for the central Makran earthquake of January 10, 1979, 15 hours. All symbols are same as Figure 7.

focal mechanism (Table 1 and Figure 19) is consistent with the first motion data (Figure 18). The 1972 sequence lies near the westernmost limit for coastal thrust events of any magnitude since the installation of the WWSSN (Figure 3).

Almost all the events we examined along the coast suggest thrust faulting and occur at depths of between 17 and 20 km. These events lie near the observed jump in acoustic velocity from 4.8 to 6.5 km/s that *White and Louden* [1982] infer to be the transition between sediments and oceanic crust (Table 4). These events presumably represent motion along the plate boundary. Two of these events (720806 and 730902) were also shown to be thrust earthquakes by Rayleigh wave analysis [*Quittmeyer and Kafka*, 1984]. One event (680803) occurred at a greater depth, 26 km, and has a well-constrained normal faulting mechanism. The other nonthrust event (800428) occurred 350 km arcward of the coast at a depth of 60 km (Table 1). This earthquake is one of the few that can be interpreted as down-dip tension events within the downgoing plate in eastern Makran. The events near the coast indicate that seismic slip begins to occur along the plate boundary at depths of about 17

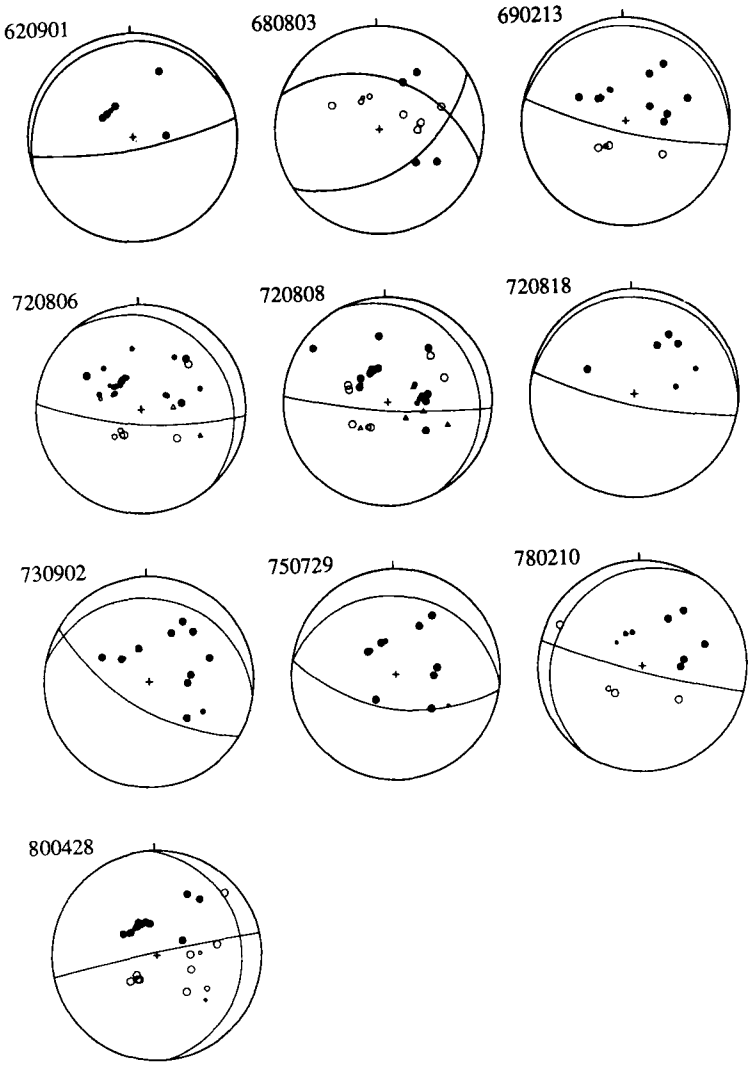

Fig. 18. Focal solutions of nine small earthquakes from first motions of P waves recorded by the World-Wide Seismic Station Network (WWSSN). Polarities read from short-period records. Lower hemisphere, equal-area projections are used; solid symbols indicate compressions; open symbols are dilatations. Symbol size proportional to quality. Most of the events are less than magnitude m_b 5.3. Focal parameters summarized in Table 1 and are shown in map view in Figure 3. Data do not tightly constrain some of these mechanisms but are sufficient to separate normal and thrust faulting events.

km, but that the plate interface remains aseismic at shallower depths. The region currently experiencing earthquakes is confined to a downdip width of about 100 km (Figure 5).

Summary of Makran Focal Solutions

The focal solutions determined in this and in previous studies are summarized in Figure 3 and Tables 1 and 2. In western Makran earthquakes with magnitudes up to M_S 6.5 occur within the subducted slab at depths of around 60 km. No thrust events, however, are observed along the interface between the colliding plates. In eastern Makran we again observe some events within the downgoing plate, but in contrast, we find that most of the seismic activity occurs along the plate boundary. The great 1945 earthquake of eastern Makran was such an event, and we have shown that it involved thrusting between the two plates. It caused 6-8 m of average slip and ruptured a region approximately 75-100 km downdip and 100-150 km along strike. Dislocation models suggest that the shallow limit of rupture was located near the coast. The large aftershock of August 5, 1947, also occurred as a thrust event along the plate boundary. A number of small thrust events continue to mark the seismogenic portion of the plate boundary along the coast of eastern Makran. These events tend to concentrate near the western limit of the 1945 rupture, but some events occur along most of the eastern coast. In central Makran much of the activity occurs along the Sistan suture zone as strike-slip deformation within the upper plate. These events probably accommodate northward motion of the Lut block relative to the Helmand block. Across the entire subduction zone a region of the plate boundary extending approximately 75 km arcward (northward) of the deformation front remains aseismic both during and between great earthquakes.

DISCUSSION

Unconsolidated Sediments Along the Plate Boundary and the Transition From Aseismic to Seismic Slip

The low-velocity portion of the accretionary wedge at the Makran subduction zone produces an aseismic zone along the

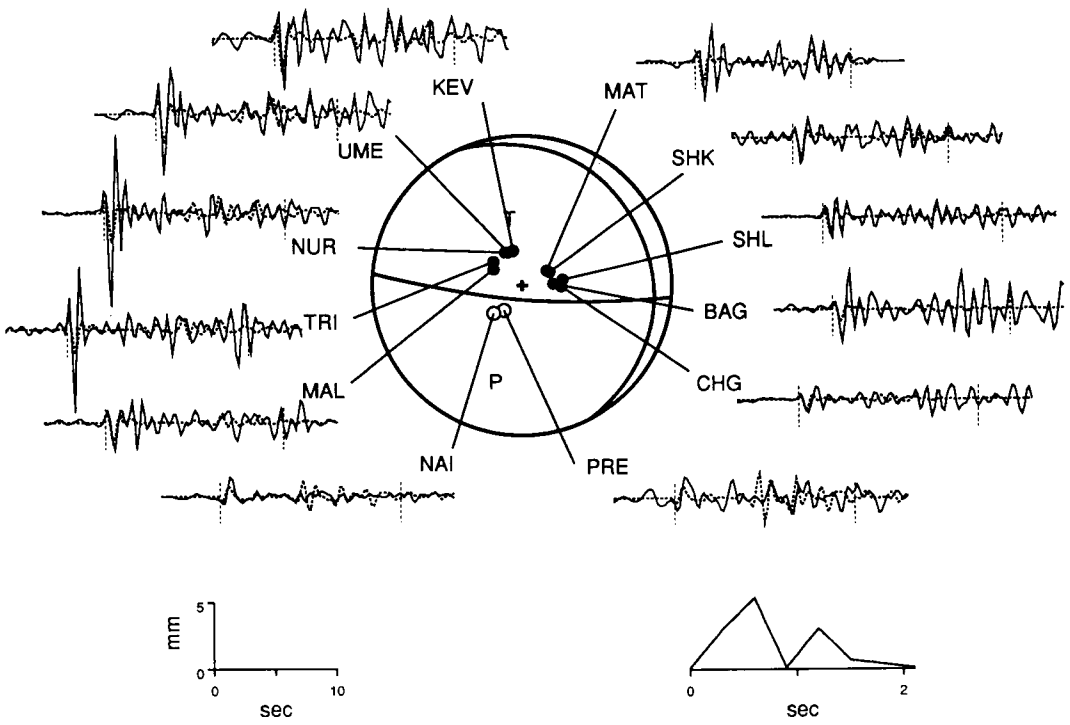

Fig. 19. Observed (solid) and synthetic (dashed) short-period seismograms for the August 8, 1972, Makran earthquake. All symbols are same as Figure 7.

shallowest part of the plate boundary very similar to that described for other subduction zones by *Byrne et al.* [1988]. Such an aseismic zone is caused by the stable sliding behavior of unconsolidated and semiconsolidated sediments along the plate interface [*Marone and Scholz*, 1988]. A transition from nonlocalized, strain-hardening to localized, strain-softening behavior occurs in a wide range of sedimentary rocks [*Zhang et al.*, 1987] with decreasing porosity and increasing confining pressure. At high pressures this transition, a prerequisite to stick-slip seismic behavior, occurs near 15-20% porosity for some relatively clay-poor sandstones [*Zhang et al.*, 1989]. Upon consolidation, slip within these rocks undergoes a transition to stick-slip motion marked by the onset of seismicity (the seismic front). The absence of seismicity suggests that the toe of the plate boundary at eastern Makran is, in fact, aseismic from the deformation front to the seismic front, a distance of about 70 km (Figure 5). As we noted previously, the abrupt change in the slope of the accretionary wedge just seaward of the seismic front in eastern Makran suggests that dewatering and underplating produce more consolidated rock within the upper plate arcward of that point. At the seismic front the sediments along the plate interface have become sufficiently dewatered to generate moderate and great thrust earthquakes in eastern Makran. The seaward limit of rupture in the great 1945 earthquake appears to occur slightly arcward of this transition in slip behavior. Dislocation models suggest that the rupture zone extends updip no more than about 30 km seaward of the coast. The absence of seismicity in western Makran does not allow us to determine the updip limit for a potential locked seismogenic zone. We suspect that if rupture were to occur there, the outermost 70 km of the plate boundary would not experience much if any slip even during a great earthquake.

Byrne et al. [1988] suggested that entirely aseismic subduction might occur in the presence of sufficiently thick sediments with low permeabilities if their unconsolidated slip properties were retained to large depths. Our findings show that aseismic slip does not persist at all depths along the plate boundary in eastern Makran. Seismic slip begins to occur where either enough time has elapsed since accretion that sufficient pore fluid has been drained to permit the required amount of consolidation of the subducted sediment or other lithified rocks are found at depth in that portion of the forearc. Very little is presently known about the velocity structure or other properties of the deeper part of the Makran forearc.

It is the amount of the plate boundary dominated by unconsolidated sediment, and hence with stable slip properties, that determines the extent of the aseismic zone. Thus the width of the aseismic zone should be roughly proportional to the amount of recently accreted, relatively unconsolidated sediment at a given forearc. The presence of a wide forearc or of a large volume of low-velocity sediment, however, does not appear in general to be sufficient to produce aseismic slip along the plate boundary at all depths. The pressures to which unconsolidated sediment will persist depends on a several factors. The most important of these are the thickness and lithology of the accreted pile. The lithology in turn controls both the presence or absence of dehydration reactions (which

can be very important in clays) and the permeability, which controls the rate at which excess pore pressures can be released. The presence of seismic slip in eastern Makran, where the sequence of incoming sediment on the subducting plate and the recently accreted portion of the forearc are both quite large, suggests that exceptional conditions must be required if any subduction zone is to undergo aseismic slip at all depths induced by sediment subduction alone.

Segmentation of the Makran Subduction Zone

For the purposes of this paper, the key differences between eastern and western Makran are the dissimilarities in seismological behavior that we described previously. The large to great earthquakes for which there are historic records have all occurred along eastern Makran (Figure 6) with the possible exception of the questionably located event of 1483. Modern seismicity exhibits this asymmetry as well (Figures 3 and 4): no thrust events are detected along the plate boundary of western Makran, while eastern Makran exhibits some plate boundary seismicity.

Segmentation is further suggested by the offsets in the volcanic arc and by the large-scale, two block structure of the overriding plate (Figure 2). The locus of volcanoes associated with subduction at Makran, shows significant offsets along the arc; *Dykstra and Birnie* [1979] suggested that Makran was broken into four segments on the basis of these offsets. One of their boundaries occurs near 61°E, coincident with the Sistan suture zone (Figure 2). The width of the region of accreted rock along the southern edge of the Helmand and Lut blocks also differs (Figure 2). A wider zone occurs south of the Helmand block [*Arthurton et al.*, 1979]. The wider accreted region in eastern Makran is consistent with the large sediment volume supplied from the east by the Indus River.

Many geologic and tectonic parameters, however, show no segmentation along the Makran subduction zone. The margin remains nearly straight for its entire 1000 km length. No ridges or other topographic features are currently being subducted west of the Murray Ridge; present marine geophysical data show no significant offsets anywhere offshore along the entire region [*White*, 1982]. The age of the subducting plate lies between approximately 70 and 100 Ma along the entire arc. Because temperature is proportional to the square root of age for seafloor created at a spreading center, as this was, the range of ages does not imply much contrast in heat flow across Makran. Variation along the arc in convergence velocity estimated from global analysis of plate motions appears to be small, with an increase of only about 6 mm/a from west to east [*DeMets et al.*, 1990].

The transitions in parameters between eastern and western Makran noted above are all approximately coincident with the Sistan suture zone, which separates the Lut and Helmand blocks (Figure 2). Seismicity and strike-slip focal solutions along the Sistan suture further support the hypothesis that the Makran subduction zone is segmented. These earthquakes indicate that at least a small amount of relative motion occurs between these blocks, with the Lut block moving northward relative to the Helmand block. The rate of relative motion between these blocks, however, appears to be small compared to the convergence along the deformation front at the southern edge of the upper plate as suggested by the absence of permanent offsets in the coast or in offshore features. Different stresses along the eastern and western strike-slip margins of Makran (Chaman-Ornach Nal and Minab, respectively) may account for the relative motion between the two blocks.

Seismic Potential for Great Earthquakes in Western Makran

Both the record of historic earthquakes and the modern seismicity (Figures 3 and 4) indicate that while most of eastern Makran has ruptured seismically and continues to be active, the plate boundary in western Makran is completely quiescent at the present and past levels of seismic monitoring. A large event in 1483 event may have struck western Makran over 500 years ago, but its location there cannot be verified. Thus the plate boundary in western Makran may experience earthquakes with longer recurrence intervals and perhaps larger magnitudes than eastern Makran, or alternatively, it may behave aseismically at all times.

Western Makran may well be entirely different from eastern Makran and experience dominantly aseismic subduction. Available data cannot confirm or reject such a hypothesis. Several conjectural mechanisms could explain such a difference in the nature of plate boundary slip. We might theorize, for instance, that the plate boundary in western Makran accommodates considerably less motion than that in the east. The relative continuity of the coast and offshore structure, however, suggest that an amount of plate convergence similar to that of eastern Makran occurs along the plate interface in western Makran. The difference in the amounts of accreted rock along the two segments might be a factor in differing styles of plate boundary slip. A shallower dip in eastern Makran might be expected from the larger volume of accreted rock [*Karig et al.*, 1976]. The plate boundary of eastern Makran does appear to have a slightly shallower dip than that of western Makran (Figure 4), which would provide a larger zone in the east that could be potentially seismogenic. In western Makran, a greater distance from the Indus River and the greater proximity to the eolian sediment source of the Arabian Peninsula suggests that the sediments accreted in the west might have a finer average grain size [*Stewart et al.*, 1965] and consequently have a lower permeability and require more time to drain. If so, these finer-grained sediments could remain unconsolidated to a greater depth along the plate boundary than the sediment in eastern Makran. Another possibility is that significant differences between the deeper portions of the forearc occur between east and west brought about by the accretion of ridges or other anomalous material. Little detail is known about the velocity structure within the Makran forearc near the coast and farther inland or about variations in the velocity structure. Better velocity data could determine whether significant differences exist. All of these mechanisms for differences in the seismic behavior between eastern and western Makran are speculative and further study is necessary to identify the causes of the dissimilarities.

The other hypothesis, that western Makran is capable of generating large to great thrust earthquakes along its plate boundary, would predict that strain energy is currently being stored to be released during future large shocks. The absence of small thrust events along the western Makran plate boundary can be interpreted as evidence of a currently locked plate boundary. The presence of young marine terraces along parts of western Makran may provide the best circumstantial evidence for great thrust earthquakes [*Page et al.*, 1979]. The processes of marine terrace formation, however, remains a problematic issue [e.g., *Fitch and Scholz*, 1971]. It cannot be

concluded that all marine terraces are formed during great earthquakes given that terraces are known to have developed from eustatic changes in sealevel alone. We also know that not all great earthquakes produce observable terraces (e.g., Chile, 1960). Geological [e.g., *Vita-Finzi*, 1982] and archaeological [e.g., *Hunting Survey Corporation*, 1960] evidence along the coast of Makran both suggest that gradual uplift occurs there. Thus, if we are to attribute Makran terraces to the occurrence of earthquakes, it is important to determine whether a given marine deposit could form from gradual or even episodic uplift or if it requires sudden or instantaneous deformation for its formation.

The only documented earthquake-associated terrace at Makran is the one at Ormara (Figure 6) that was formed by the 1945 earthquake. This event elevated a pre-1945 wave-cut platform 2 m above the present one [*Page et al.*, 1979]. Other terraces are identified at Ormara and at several localities in western Makran, in particular at Konarak (Figure 6). Only two marine terraces younger than 6000 years occur in western Makran. Both of these terraces (T1 and T2 of *Page et al.* [1979]) are preserved as small remnants. *Vita-Finzi* [1980, 1981] dated shells at other localities that have been uplifted, but they are either not from terraces (e.g., shells out of growth position from a beach deposit buried by alluvium) or are much older. The two young terraces postdate all possible high sea level stands during the Pleistocene [*Fairbanks*, 1989]; consequently, they seem to demand a tectonic generating mechanism for their uplift with respect to a relatively steady sealevel. Although these terraces may have been produced during earthquakes, this conclusion is not clearly established. A number of other terraces in western Makran, with considerably greater ages, create steps reaching elevations of up to 105 m [*Page et al.*, 1979].

Average Repeat Times and Future Makran Events

The damage caused by the large historic events of eastern Makran suggests that they, like the 1945 shock, were thrust events along the plate boundary. Felt reports indicate that the older sequences were probably not as large as the 1945 earthquake. Thus none were large enough to rupture more than 150-200 km along the strike of the subduction zone. The large distances between towns damaged by these three events suggests that each ruptured a different section of the plate boundary. Thus the historic earthquakes do not enable us to directly estimate the average repeat time for events within any given segment. Using Holocene uplift rates along the Makran coast inferred from marine terraces and assuming such uplift occurs during earthquakes, *Page et al.* [1979] estimates average repeat times of 1000-2000 years in the 1945 zone and 3000-20,000 years in western Makran. These long time intervals suggest that either most of the plate motion is accommodated aseismically or that not all great earthquakes cause terraces at the same place. Because the historic record is complete for great events across all of Makran since at least the mid-nineteenth century [*Ambraseys and Melville*, 1982], we can make estimates of the minimum repeat times. The historic record suggests that at least 140 years elapsed between events in the 1851/1864 region and more than 200 years in the 1765 zone. We also know that at least 100 years passed without great events in the 1945 zone prior to that earthquake. We infer from dislocation models that slip of approximately 7 m occurred in 1945. If all of the plate motion between Eurasia and Arabia occurred during earthquakes like 1945, such events would be expected to recur at least every 175 years. Because most subduction zones experience at least some aseismic slip [*Sykes and Quittmeyer*, 1981; *Peterson and Seno*, 1984], events like 1945 would be expected to occur even less frequently. Also, if the long-term rate of movement along the Makran subduction zone is, in fact, more like half of that for Arabia-Eurasia, the repeat time for the 1945 zone could be greater than 300 years.

The absence of large to great historic events does not allow us to estimate a repeat time for potential large earthquakes in western Makran. The 1483 earthquake may have occurred in western Makran, but it is misleading to presume that the region has not experienced any large or great earthquakes since then. The historic record in western Makran is probably only as complete as that of eastern Makran, so we are merely able to say that at least 140 years have passed without any large events occurring there. If we assume that the full rate of convergence calculated between the Arabian and Eurasian plates occurs along the Makran plate interface and further assume that all of it is released during great earthquakes and that none have occurred since 1483, then the accumulated motion along the plate boundary of western Makran since 1483 amounts to approximately 18 m. We suggest that all of these assumptions are not likely to be valid and that any accumulated strain energy will be considerably less. Assuming that the convergence rate for Makran is half of the Arabian-Eurasian rate, the possible accumulated slip is about 9 m since 1483, about equivalent to a shock of M_w 8.5. We do not know if western Makran could rupture at all in a large or great earthquake, and if so, whether it would be more likely to break in a single great event or in a series of somewhat smaller magnitude shocks.

Recent seismicity (Figures 1 and 3) clusters at the western end of the 1945 rupture zone and at the western end of the inferred 1851 rupture area. These clusters are separated by a region with less seismicity (Figure 3). This seismicity pattern led *Quittmeyer* [1979] to speculate that the region immediately to the west of the 1945 zone may be nearing a repeat of the 1851 earthquake sequence. The largest Makran earthquake (m_b 6.5) since the installation of the WWSSN occurred as a downdip tensional event in the lower plate arcward of this quiet region [*Laane and Chen*, 1989] adding further evidence of accumulating stresses within that segment of the Makran subduction zone.

Implications for Other Subduction Zones

The implications of this study fit into the larger question of assessment of the seismic potential at subduction zones that have experienced few or no plate boundary earthquakes historically. We have shown that western Makran may be interpreted as either an aseismic subduction zone or as one that is currently (and has remained throughout historic times) completely locked. The latter hypothesis obviously implies a potentially great seismic hazard. There are several other subduction zones that have no historic record of great earthquakes. In some cases, such as the Marianas subduction zone, a combination of large slab age and a low rate of convergence is commonly thought to cause a low potential for great events thereby explaining their absence [e.g., *Ruff and Kanamori*, 1983]. However, at margins with no historic events, younger slabs and greater convergence rates, such a model suggests that great earthquakes should have or will occur. In the case of Makran, differences in age and convergence rate appear unable to explain the dramatic differences in seismic behavior between the eastern and western

segments. Like western Makran, the Cascadia subduction zone of North America may be somewhat enigmatic. Geologic evidence at Cascadia, most notably the presence of sudden subsidence events along the coast, has been interpreted as evidence of prehistoric earthquakes [e.g., *Atwater*, 1987], with current ^{14}C dates indicating that the last subsidence event correlated between at least two estuaries occurred around 300 years ago [*Atwater and Stuiver*, 1991]. The complete absence of thrust earthquakes at Cascadia would then be explained as evidence of complete locking of the entire margin, which then breaks in great earthquakes with long repeat times [e.g., *Heaton and Kanamori*, 1984]. The Cascadia margin exhibits segmentation in several geological and geophysical aspects, however, and *Sykes et al.* [1987] have suggested that the complete absence of thrust earthquakes of any size on any of these segments during the historic record is highly anomalous. It remains to be seen which other factors [e.g., *Peterson and Seno*, 1984] are able to explain deviations from the traditional age-rate models and the wide variations in seismic behavior such as that observed at Makran.

CONCLUSIONS

The Makran subduction zone of eastern Iran and southwestern Pakistan has a relatively low level of seismicity with few earthquakes sufficiently large for source parameter determination and infrequent large or great events. Consequently, the seismic behavior of Makran has remained poorly known. One of the primary purposes of this paper has been to analyze that behavior. We determined the source parameters for as many small to great earthquakes as possible (14 events) to investigate that behavior. We focused, in particular, on the great earthquake of 1945, because it is the only instrumentally recorded great event at Makran, it represents 95% of the seismic moment released along the subduction zone during this century, and its source parameters were not determined prior to our study. A second aspect of this study has been to examine the effects of accretion and subduction of large amounts of young sediment on the style of slip along the plate boundary and on the potential for generating great thrust earthquakes.

We found that the great (M_W 8.1) earthquake of November 27, 1945, is a thrusting event along an eastern segment of the plate boundary. We employed body waveform modeling, first motions of bodywaves, surface wave analysis, and dislocation modeling to constrain the source parameters. We also found that the large (M_S 7.3) aftershock of 1947 occurred as thrusting along the plate boundary. The scalar seismic moment determined for the 1945 event is 1.8×10^{21} N m based on mantle Rayleigh waves corresponding to a moment magnitude of M_W 8.1. Dislocation models, body waveform inversion, and moment estimates suggest that the earthquake ruptured less than 200 km along the arc (at most one-fifth of the arc length) and approximately 100 km in a downdip direction. Our preferred source time function consists of three pulses growing in amplitude and duration with a total duration of about 56s. The initial pulse is quite small, leading to some difficulty in picking the initial motion of body waves at stations with low magnification or higher noise levels. This difficulty makes the first motion of P waves data somewhat suspect. Body waveform analysis indicates that the rupture began at a depth near 30 km and propagated updip and eastward. Dislocation models of the coastal uplift associated with this earthquake suggest that updip rupture along the décollement continued seaward to the vicinity of the coast but did not rupture more than approximately 30 km seaward of it. The downdip limit of rupture appears shallow compared to other subduction zones. It is possible, however, that the event ruptured a longer downdip segment and a shorter distance along strike than we have inferred.

We found thrust faulting focal solutions for eight additional Makran earthquakes with depths at or near the plate boundary. All of these thrust events are confined to eastern Makran. The seismogenic part of the plate boundary delineated by these events is approximately 100 km in downdip width. It extends seaward about 50 km beyond the coast. Downdip rupture during the 1945 earthquake nearly coincides with the currently active part of the plate boundary. The shallow limit of plate boundary seismicity, the seismic front, occurs at a depth of about 17 km. Farther seaward an aseismic zone extends an additional 75 km out to the deformation front. This aseismic zone appears to remain aseismic both during and between great earthquakes.

Modern seismicity, the historical record of larger events, and our focal solutions show strong segmentation in the Makran subduction zone between eastern and western segments. Much of eastern Makran appears to have ruptured within the last 225 years in large or great earthquakes and small- and moderate-sized plate boundary earthquakes continue to occur. In contrast, the plate boundary of western Makran has no established record of large or great plate boundary events in historic times nor have any such events of any size been detected by more recent seismic monitoring. Nearly all of the earthquakes occurring in the western segment are of intermediate depth and represent normal faulting within the downgoing plate. The segmentation is also apparent in the large-scale structure of the upper plate; it is made up of two older continental blocks with younger rock accreted along their southern margins. The volume of accreted rock is greater in eastern Makran and the sediments supplied to western Makran are on average somewhat more fine grained. In central Makran we determined strike-slip focal solutions for two events that occurred within the upper plate between these blocks. The earthquakes indicate that the western, Lut, block moves northward to some extent relative to the eastern, Helmand, block but the continuity of the coastline and of offshore structures indicates that their long-term motions must be similar. The volcanic arc is offset between the two segments; a greater distance occurs between the deformation front and the arc in eastern Makran. The alignment between the transitions in seismicity and the boundary between these blocks suggests that the difference in seismic behavior is related to the segmentation of the upper plate. Differences between the motions of the Lut and Helmand blocks may be caused by the very dissimilar fault zones along the boundaries of eastern and western Makran.

No thrust events are known to occur along the plate boundary of western Makran. Thus its long-term seismic behavior and its potential for great earthquakes are unknown. We are faced with the extreme alternatives of a completely locked plate boundary or of largely aseismic subduction. The occurrence of uplifted Holocene marine terraces along the coast and the apparent continuity of convergence velocity between eastern and western Makran suggest that the absence of seismic activity is best interpreted as a locked plate boundary rather than as aseismic subduction. The data concerning the seismic behavior in western Makran are not sufficient for us to make any estimates concerning the timing or the rupture extent of a potential earthquake.

Makran is a subduction zone with an enormous amount of accreted rock including a very wide toe of recently accreted, largely unconsolidated sediment. Such unconsolidated sediments exhibit stable slip properties resulting in aseismic behavior. In eastern Makran the outermost 70 km of the plate boundary lies within such sediment and remains aseismic. The stable slip properties of unconsolidated sediment led *Byrne et al.* [1988] to speculate that massive subduction of young sediment might reduce the seismic potential of a subduction zone. Our analysis of eastern Makran indicates that there the accreted and subducted sediment becomes sufficiently dewatered and consolidated to generate great plate boundary earthquakes.

The implications of this study are important for the assessment of the seismic potential along the coast of eastern and western Makran as well as for other margins with abundant sediments and few or no plate boundary earthquakes. This study shows that a large sediment volume does not necessarily indicate a low potential for great thrust earthquakes.

Acknowledgments. We are indebted to J. Pacheco for assistance with computer programs and for many beneficial suggestions and discussions throughout this study and to C. Estabrook for helpful discussions as well as assistance in our surface wave investigation. We thank J. Beavan for providing his dislocation modeling program. W.-P. Chen, R. Quittmeyer, J. Mori, J. P. McCaffrey, and others provided historic seismograms. We thank C. Scholz, M. Langseth, and three anonomous reviewers for helpful reviews of the manuscript and W.-P. Chen and B. Atwater for additional comments. This research was supported by the National Science Foundation under grant EAR87-07719. Lamont-Doherty contribution 4849.

REFERENCES

Abe, K., Magnitudes of large shallow earthquakes form 1904 to 1980, *Phys. Earth Planet. Inter.*, *27*, 72-92, 1981.

Ahmed, S. S., Tertiary geology of part of south Makran, Baluchistan, West Pakistan, *Am. Assoc. Pet. Geol. Bull.*, *53*, 1480-1499, 1969.

Aki, K., and P. G. Richards, *Quantitative Seismology, Theory and Methods*, 932 pp., W. H. Freeman, New York, 1980.

Ambraseys, N. N., and C. P. Melville, *A History of Persian Earthquakes*, 219 pp., Cambridge University Press, New York, 1982.

Arthurton, R. S., G. S. Alam, S. Anisuddin-Ahmad, and S. Iqbal, Geological history of the Alamreg-Mashki Chah area, Chagai district, Baluchistan, in *Geodynamics of Pakistan*, edited by A. Farah and K. A. de Jong, pp. 325-331, Geological Survey of Pakistan, Quetta, 1979.

Atwater, B. F., Evidence for great Holocene earthquakes along the outer coast of Washington State, *Science*, *236*, 942-944, 1987.

Atwater, B. F., and M. Stuiver, Precise ^{14}C ages for sudden Holocene submergence in Washington, *Geol. Soc. Am. Abstr. Programs*, *23*, 4, 1991.

Banghar, A. R., and L. R. Sykes, Focal mechanisms of earthquakes in the Indian Ocean and adjacent regions, *J. Geophys. Res.*, *74*, 632-649, 1969.

Barrientos, S. E., and S. N. Ward, The 1960 Chile earthquake: Inversion for slip distribution from surface deformation, *Geophys. J. Int.*, *103*, 589-598, 1990.

Boyd, T. M., and J. L. Nábělek, Rupture process of the Andreanof Islands earthquake of May 7, 1986, *Bull. Seismol. Soc. Am.*, *78*, 1653-1673, 1988.

Byrne, D. E., L. R. Sykes, and D. M. Davis, Loci and maximum size of thrust earthquakes and the mechanics of the shallow region of subduction zones, *Tectonics*, *7*, 833-857, 1988.

Byrne, D. E., L. R. Sykes, and D. M. Davis, The great Makran earthquake of 1945 and its implications for modes of plate boundary slip (abstract), *Eos Trans. AGU*, *70*, 1330, 1989.

Chandra, U., Focal mechanism solutions for earthquakes in Iran, *Phys. Earth Planet. Inter.*, *34*, 9-16, 1984.

Charlier, C., and J. M. van Gils, *Liste des Stations Séismologiques Mondiales*, Observatoire Royal de Belgique, Uccle, 1953.

Choy, G. L., and P. G. Richards, Pulse distortion and Hilbert transformation in multiply reflected and refracted body waves, *Bull. Seismol. Soc. Am.*, *65*, 55-70, 1975.

Coleman, R. G., Tectonic setting for ophiolite obduction in Oman, *J. Geophys. Res.*, *86*, 2497-2508, 1981.

Collier, J. S., and R. S. White, Mud diapirism within Indus fan sediments: Murray Ridge, Gulf of Oman, *Geophys. J. Int.*, *101*, 345-353, 1990.

Davis, D., J. Suppe, and F. A. Dahlen, Mechanics of fold-and-thrust belts and accretionary wedges, *J. Geophys. Res.*, *88*, 1153-1172, 1983.

DeMets, C., R. G. Gordon, D. F. Argus, and S. Stein, Current plate motions, *Geophys. J. Int.*, *101*, 425-478, 1990.

Duda, S. J., Secular seismic energy release in the circum-Pacific belt, *Tectonophysics*, *2*, 409-452, 1965.

Dziewonski, A. M., A. Friedman, D. Giardini, and J. H. Woodhouse, Global seismicity of 1982: Centroid-moment tensor solutions for 308 earthquakes, *Phys. Earth Planet. Inter.*, *33*, 76-90, 1983.

Dykstra, J. D., and R. W. Birnie, Segmentation of the Quaternary subduction zone under the Baluchistan region of Pakistan and Iran, in *Geodynamics of Pakistan*, edited by A. Farah and K. A. de Jong, pp. 319-323, Geological Survey of Pakistan, Quetta, 1979.

Fairbanks, R. G., A 17000-year glacio-eustatic sea level record: influence of glacial melting rates on the Younger Dryas event and deep-ocean circulation, *Nature*, *342*, 637-642, 1989.

Farhoudi, G., A comparison of Zagros geology to island arcs, *J. Geol.*, *86*, 323-334, 1978.

Farhoudi, G., and D. E. Karig, Makran of Iran and Pakistan as an active arc system, *Geology*, *5*, 664-668, 1977.

Fitch, T. J., and C. H. Scholz, Mechanism of underthrusting in southwest Japan: A model of convergent plate interactions, *J. Geophys. Res.*, *76*, 7260-7292, 1971.

Fowler, S. R., R. S. White, and K. E. Louden, Sediment dewatering in the Makran accretionary prism, *Earth Planet. Sci. Lett.*, *75*, 427-438, 1985.

Geller, R. J., and H. Kanamori, Magnitudes of great shallow earthquakes from 1904 to 1952, *Bull. Seismol. Soc. Am.*, *67*, 587-598, 1977.

Gordon, R., and C. DeMets, Present-day motion along the Owen fracture zone and Dalrymple trough in the Arabian Sea, *J. Geophys. Res.*, *94*, 5560-5570, 1989.

Gutenberg, B., and C. F. Richter, *Seismicity of the Earth and Associated Phenomena*, 310 pp., Princeton University Press, Princeton, N.J., 1954.

Haghipour, A., M. Ghorashi, and M. H. Kadjar, Explanatory text of the seismotectonic map of Iran, Afghanistan and Pakistan, Commission for geological map of world-UNESCO, Geol. Surv. of Iran, Tehran, 1984.

Harms, J. C., H. N. Cappel, and D. C. Francis, The Makran coast of Pakistan: its stratigraphy and hydrocarbon potential, in *Marine Geology and Oceanography of Arabian Sea and Coastal Pakistan*, edited by B. U. Haq and J. D. Milliman, pp. 3-26, Van Nostrand Reinhold, *Co.*, New York, 1984.

Heaton, T. H., and H. Kanamori, Seismic potential associated with subduction in the northwestern United States, *Bull. Seismol. Soc. Am.*, *74*, 933-941, 1984.

Herrin, E., Seismological tables for *P* phases, *Bull. Seismol. Soc. Am.*, *58*, 1193-1239, 1968.

Hunting Survey Corporation, *Reconnaissance Geology of Part of West Pakistan: A Colombo Pan Co-operative Project*, 550 pp., Maracle Press, Toronto, Ont., 1960.

Hutchison, I, K. E. Louden, R. S. White, and R. P. von Herzen, Heat flow and age of the Gulf of Oman, *Earth Planet. Sci. Lett.*, 56, 252-262, 1981.

Isacks, B. L., and M. Barazangi, Geometry of Benioff zones: Lateral segmentation and downwards bending of the subducted lithosphere, in *Island Arcs, Deep Sea Trenches and Back-Arc Basins, Maurice Ewing Ser.*, vol. 1, edited by M. Talwani and W. C. Pitman III, pp. 99-114, AGU, Washington, D. C., 1977.

Jackson, J., and D. McKenzie, Active tectonics of the Alpine-Himalayan Belt between Turkey and Pakistan, *Geophys. J. R. Astron. Soc.*, *77*, 185-264, 1984.

Jacob, K. H., and R. L. Quittmeyer, The Makran region of Pakistan and Iran: trench-arc system with active plate subduction, in *Geodynamics of Pakistan*, edited by A. Farah and K. A. de Jong, pp. 305-317, Geological Survey of Pakistan, Quetta, 1979.

Kadinsky-Cade, K., and M. Barazangi, Seismotectonics of southern Iran: The Oman Line, *Tectonics*, *1*, 389-412, 1982.

Kanamori, H., Importance of historical seismograms for geophysical research, in *Historical Seismograms and Earthquakes of the World*,

edited by W. H. K. Lee, H. Meyers and K. Shimazake, pp. 16-33, Academic, San Diego, Calif., 1988.

Karig. D. E., J. G. Caldwell, and E. M. Parmentier, Effects of accretion on the geometry of the descending lithosphere, *J. Geophys. Res.*, *81*, 6281-6291, 1976.

Laane, J., and W. P. Chen, The Makran earthquake of 1983 April 18: A possible analogue to the Puget Sound earthquake of 1965?, *Geophys. J. Int.*, *98*, 1-9, 1989.

Lerner-Lam, A. L., and T. H. Jordan, Earth structure from fundamental and higher-mode waveform analysis, *Geophys. J. R. Astron. Soc.*, *75*, 759-797, 1983.

Marone, C., and C. H. Scholz, The depth of seismic faulting and the upper transition from stable to unstable slip regimes, *Geophys. Res. Lett.*, *15*, 621-624, 1988.

McCall, G., and R. Kidd, The Makran, southeastern Iran: The anatomy of a convergent plate margin active from Cretaceous to Present, in Trench-Forearc Geology: Sedimentation and Tectonics on Modern and Ancient Active Plate Margins, edited by J. K. Leggett, *Geol. Soc. Spec. Publ. London*, *10*, 387-397, 1982.

McComb, H. E., and C. J. West, *List of Seismological Stations of the World*, 2nd ed., *Bull. Nat. Res. Counc.*, *82*, 119 pp., 1931.

Milliman, J. D., G. S. Quraishee, and M. A. A. Beg, Sediment discharge from the Indus River to the ocean: past, present and future, in *Marine Geology and Oceanography of Arabian Sea and Coastal Pakistan*, edited by B. U. Haq and J. D. Milliman, pp. 65-70, Van Nostrand Reinhold, New York, 1984.

Minshull, T., and R. White, Sediment compaction and fluid migration in the Makran accretionary prism, *J. Geophys. Res.*, *94*, 7387-7402, 1989.

Mocquet, A., B. Romanowicz, and J. P. Montagner, Three-dimensional structure of the upper mantle beneath the Atlantic Ocean inferred from long-period Rayleigh waves, 1, Group and phase velocity distributions, *J. Geophys. Res.*, *94*, 7449-7468, 1989.

Molnar, P., Continental tectonics in the aftermath of plate tectonics, *Nature*, *335*, 131-137, 1988.

Nábělek, J., Determination of earthquake source parameters from inversion of body waves, Ph.D. Thesis, 360 pp., Mass. Inst. of Technol., Cambridge, 1984.

Nábělek, J., Geometry and mechanism of faulting of the 1980 El Asnam, Algeria earthquake from inversion of teleseismic body waves and comparison with field observations, *J. Geophys. Res.*, *90*, 12,713-12,728, 1985.

Nábělek, J., and G. Suárez, The 1983 Goodnow earthquake in the central Adirondacks, New York: Rupture of a simple, circular crack, *Bull. Seismol. Soc. Am.*, *79*, 1762-1777, 1989.

Niazi, M., H. Shimamura, and M. Matsu'ura, Microearthquakes and crustal structure off the Makran coast of Iran, *Geophys. Res. Lett.*, *7*, 297-300, 1980.

Nowroosi, A. A., Focal mechanism of earthquakes and plate tectonics of Middle East, *Bull. Seismol. Soc. Am.*, *62*, 823-850, 1972.

Oldham, J., A catalogue of Indian earthquakes, *Mem. Geol. Surv. India*, *19*, 163-215, 1882.

Okal, E. A., A theoretical discussion of time domain magnitudes: the Prague formula for M_S and the mantle magnitude M_m, *J. Geophys. Res.*, *94*, 4194-4204, 1989.

Okal, E. A., and J. Talandier, M_m: A variable-period mantle magnitude, *J. Geophys. Res.*, *94*, 4169-4193, 1989.

Page, W. D., J. N. Alt, L. S. Cluff, and G. Plafker, Evidence for the recurrence of large-magnitude earthquakes along the Makran coast of Iran and Pakistan, *Tectonophysics*, *52*, 533-547, 1979.

Pendse, C. G., The Makran earthquake of the 28th of November, 1945, Sci. Notes, *10*, pp. 141-145, Indian Meterol. Dep., 1948.

Peterson, E. T., and T. Seno, Factors affecting seismic moment release rates in subduction zones, *J. Geophys. Res.*, *89*, 10,233-10,248, 1984.

Plafker, G., Alaskan earthquake of 1964 and Chilean earthquake of 1960: Implications for arc tectonics, *J. Geophys. Res.*, *77*, 901-925, 1972.

Platt, J. P., Thrust mechanics in highly overpressured accretionary wedges, *J. Geophys. Res.*, *95*, 9025-9034, 1990.

Platt, J. P., J. K. Leggett, J. Young, H. Raza, and S. Alam, Large-scale sediment underplating in the Makran accretionary prism, southwest Pakistan, *Geology*, *13*, 507-511, 1985.

Platt, J. P., J. K. Leggett, and S. Alam, Slip vectors and fault mechanics in the Makran accretionary wedge, southwest Pakistan, *J. Geophys. Res.*, *93*, 7955-7973, 1988.

Quittmeyer, R. C., Seismicity variations in the Makran region of Pakistan and Iran: Relation to great earthquakes, *Pure Appl. Geophys.*, *117*, 1213-1228, 1979.

Quittmeyer, R. C., and K. H. Jacob, Historical and modern seismicity of Pakistan, Afghanistan, northwestern India, and southeastern Iran, *Bull. Seismol. Soc. Am.*, *69*, 773-823, 1979.

Quittmeyer, R. C., and A. L. Kafka, Constraints on plate motions in southern Pakistan and the northern Arabian Sea from the focal mechanisms of small earthquakes, *J. Geophys. Res.*, *89*, 2444-2458, 1984.

Ruff, L., and H. Kanamori, Seismic coupling and uncoupling at subduction zones, *Tectonophysics*, *99*, 99-117, 1983.

Sengör, A.M. C., D. Altiner, A. Cin, T. Ustaömer, and K. J. Hsü, Origin and assembly of the Tethyside orogenic collage at the expense of Gondwana Land, in Gondwana and Tethys, edited by M. G. Audley-Charles and A. Hallam, *Geol. Soc. London Spec. Publ. 37*, 119-181, 1988.

Snead, R. L., Active mud volcanoes of Baluchistan, West Pakistan, *Geog. Rev.*, *54*, 546-560, 1964.

Sohon, F. W., *Theoretical Seismology, Part 2*, 149 pp., John Wiley, New York, 1932.

Sondhi, V. P., The Makran earthquake, 28th November 1945: The birth of new islands, *Indian Miner.*, *1*, 147-154, 1947.

Stein, S., E. A. Okal, and D. A. Wiens, Application of modern techniques to analysis of historical earthquakes, in *Historical Seismograms and Earthquakes of the World*, edited by W. H. Lee, H. Meyers, and K. Shimazaki, pp. 85-104, Academic, San Diego, Calif., 1988.

Stewart, R. A., O. H. Pilkey, and B. W. Nelson, Sediments of the northern Arabian Sea, *Mar. Geol.*, *3*, 411-427, 1965.

Sykes, L. R., and R. L. Quittmeyer, Repeat times of great earthquakes along simple plate boundaries, in *Earthquake Prediction: An International Review, Maurice Ewing Ser.*, vol. 4, edited by D. W. Simpson and P. G. Richards, pp. 217-247, AGU, Washington, D. C., 1981.

Sykes, R. L., D. E. Byrne, and D. M. Davis, Seismic and aseismic subduction: Aseismic slip at zones of massive sediment supply and the nature of great asperities at convergent margins, *Eos, Trans. AGU*, *68*, 1468, 1987.

Tilton, G. R., C. A. Hopson, and J. E. Wright, Uranium-Lead isotopic ages of the Samail ophiolite, Oman, with applications to Tethyan ocean ridge tectonics, *J. Geophys. Res.*, *86*, 2763-2775, 1981.

Tippit, P. R., E. A. Pessagno, Jr., and J. D. Smewing, The biostratigraphy of sediments in the volcanic unit of the Samail ophiolite, *J. Geophys. Res.*, *86*, 2756-2762, 1981.

Tirrul, R., I. R. Bell, R. J. Griffis and V. E. Camp, The Sistan suture zone of eastern Iran, *Geol. Soc. Am. Bull.*, *94*, 134-150, 1983.

Vita-Finzi, C., ^{14}C dating of recent crustal movements in the Persian Gulf and Iranian Makran, *Radiocarbon*, *22*, 763-773, 1980.

Vita-Finzi, C., Late Quaternary deformation on the Makran coast of Iran, *Z. Geomorphol.*, suppl., *40*, 213-226, 1981.

Vita-Finzi, C., Recent coastal deformation near the Strait of Hormuz, *Proc. R. Soc. London, Ser. A*, *382*, 441-457, 1982.

von Huene, R., Tectonic processes along the front of modern convergent margins–Research of the past decade, *Anu. Rev. Earth Planet. Sci.*, *12*, 359-381, 1984.

White, R. S., Deformation of the Makran continental margin, in *Geodynamics of Pakistan*, pp. 295-304, edited by A. Farah and K. A. de Jong, Geological Survey of Pakistan, Quetta, 1979.

White, R. S., Deformation of the Makran accretionary sediment prism in the Gulf of Oman, in Trench-Forearc Geology: Sedimentation and Tectonics on Modern and Ancient Active Plate Margins, edited by J. K. Leggett, *Geol. Soc. Spec. Publ. London*, *10*, 357-372, 1982.

White, R. S., The little Murray Ridge, in *Seismic Expression of Structural Styles*, edited by A. W. Bally, pp. 1.3.10-1.3.23, American Association Petroleum Geologists, Tulsa, Okla., 1983.

White, R. S., Active and passive plate boundaries around the Gulf of Oman, north-west Indian Ocean, *Deep Sea Res.*, *31*, 731-745, 1984.

White, R. S. and K. E. Louden, The Makran continental margin: structure of a thickly sedimented convergent plate boundary, in Studies in Continental Margin Geology, edited by J.S. Watkins and C. L. Drake, *AAPG Mem.*, *34*, 499-518, 1982.

White, R. S., and K. Klitgord, Sediment deformation and plate tectonics in the Gulf of Oman, *Earth Planet. Sci. Lett.*, *32*, 199-209, 1976.

White, R. S., and D. A. Ross, Tectonics of the western Gulf of Oman, *J. Geophys. Res.*, *84*, 3479-3489, 1979.

Woodhouse, J. H., and A. M. Dziewonski, Three-dimensional modeling

of Earth structure by inversion of seismic waveforms, *J. Geophys. Res.*, *89*, 5953-5986, 1984.

Zhang, J., T.-f. Wong, and D. M. Davis, Failure modes as a function of porosity and effective pressure in porous sandstone (abstract), *Geol. Soc. Am. Abstr. Programs.*, *19*, 904, 1987.

Zhang, J., T.-f. Wong, and D. M. Davis, The brittle to ductile transition in porous sandstone (abstract), *Eos Trans. AGU*, *70*, 1360, 1989.

D.E. Byrne, Instituto de Geofisica, Universidad Nacional Autónoma de México, Cindad Universitaria, Delegación de Coyoacar, Apdo. Postal 21-499, 04000 México, D.F., Mexico.

D.M. Davis, Department of Earth and Space Sciences, SUNY Stony Brook, Stony Brook, N Y 11794.

L.R. Sykes, Lamont-Doherty Geological Observatory of Columbia University, Palisades, N Y 10964.

(Received October 26, 1990;
revised July 22, 1991;
accepted August 12, 1991.)